



Implication of deformation fabrics of schist-migmatite-gneiss and granite in understanding regional tectonics: Eastern Dharwar Craton (EDC), India

Sukanta Goswami¹ · Sangeeta Bhagat¹ · Dheeraj Pande¹ · D. K. Choudhury¹ · B. Saravanan¹ · D. K. Sinha¹

Received: 19 December 2022 / Accepted: 6 May 2023 / Published online: 2 June 2023
© Indian National Science Academy 2023

Abstract

Structural fabrics of schist belt, gneiss, migmatites and younger granitoids are different. Various morphology of migmatites is recognized for the first time in the southern part of EDC along with gneiss. The younger granite plutons are examined from northern through central to southern part of EDC. The paleosome-dominated portions of migmatite were possibly formed from low degree partial melting of older rocks and identified as metatexites. Whereas, the neosome dominated parts were developed by complete melting and marked as diatexites. There is a link between diatexite and granite in the southern part, which is characterized as catazone segment. The four sub-types of metatexites are observed (viz, patch, dilatant, net and stromatic). The diatexites are dominated by two major structures (viz, schollen or raft and schlieren). Gneisses show lit-per-lit as well as fold and leucocratic material flow features. The litho-structural variation from north to south connotes systematic changes from epizone through mesozone to catazone. The qualitative study of mineral content and textural aspects from rocks at different localities suggest preserved portions of different parts of a pressure–temperature path. However, exact quantification should be possible after thermo-barometry and pseudo section study. The present contribution focuses on documentation of classic representative outcrops and petrographic features of gneissic and migmatitic rocks of EDC. It is observed that the six (6) major ductile deformation stages of Kenoran orogeny implies ductile signature before granite plutonism. Subsequently post granite emplacement deformation phenomenon indicates a transition from ductile to brittle regime and entrance into Hudsonian orogeny.

Keywords Structural attributes · Partial melting · Eastern Dharwar Craton (EDC) · Types of migmatite

Introduction

Dharwar Craton (DC) is one of the oldest parts of the Earth's continental crust that remain stable inside the Indian plate since Archaean (Jayananda et al. 2018, 2023; Goswami et al. 2021a). The DC has mainly three major tectonic domains (1. > 3.2 Ga cratonic nuclei with Late Archaean younger granite plutons, 2. Proterozoic mobile belt, 3. Proterozoic basins). Recently the DC is divided into three cratonic blocks (i.e., east, central and west blocks after Peucat et al. 2013; Jayananda et al. 2018, 2020; Dey 2013; Li et al. 2018a, b)

on the basis of age relationships of rocks, thermal records and interpreted accretionary histories. However, most of the literature suggests about two major components viz., East Dharwar Craton (EDC) and West Dharwar Craton (WDC) on the basis of contrasts in lithounits, metamorphic grade and crustal thickness (Fig. 1). The Chitradurga shear zone (CSZ) has been considered as dividing plane between the EDC and WDC (Naqvi and Rogers 1987; Chadwick et al. 1996, 2000, 2007; Chardon et al. 2008, 2011; Jayananda et al. 2006, 2015). Some literature considers Closepet Granite (CG) as the contact area between these two blocks (e.g., Swami Nath et al. 1976; Vishwanatha and Ramakrishnan 1976; Swami Nath and Ramakrishnan 1981; Moyen et al. 2003; Gupta et al. 2003).

In this context, it must be noted that these Archaean rocks of DC form the basement for three Proterozoic basins viz, Cuddapah, Bhima and Kaladgi basins. Among these Kaladgi basin comes under both EDC and WDC. Two cratons cannot

✉ Sukanta Goswami
sukantagoswami.amd@gov.in

¹ Atomic Minerals Directorate for Exploration and Research, Headquarter, 7-201, Divyashakti Apartment, Hyderabad, Telangana 500016, India

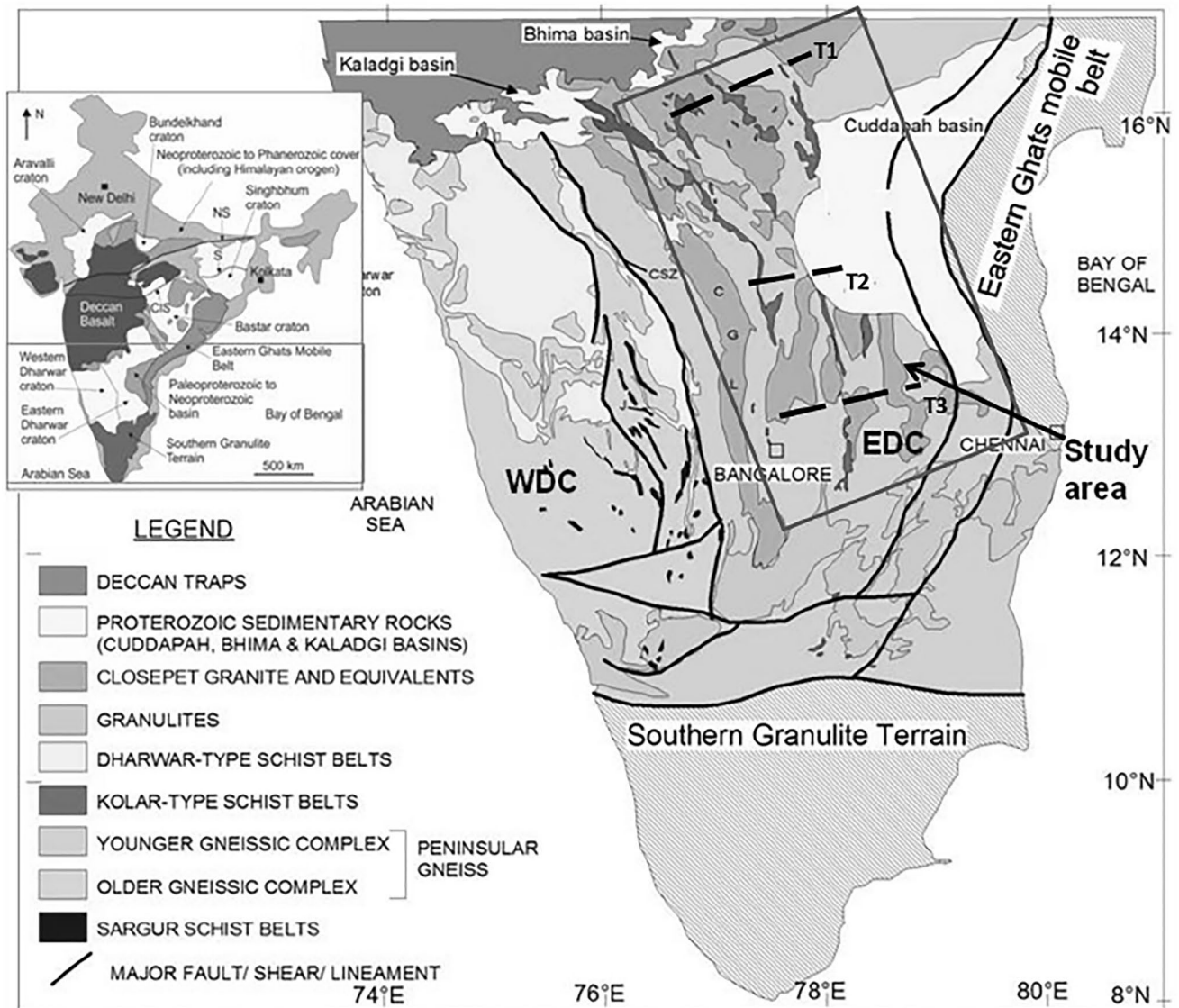


Fig. 1 Geological map of the Dharwar Craton, Southern India (modified after Vasundhara Project, Geological Survey of India 1994). T1, T2 and T3 represents major transacts in the northern, central and southern part of EDC

comprise same platformal basin and it is not so far common to introduce inter cratonic basin. Usually mobile belts exist in between two cratons (Katz 1985) but there are no such mobile belts in between EDC and WDC. Thus, instead of considering the EDC and WDC as different cratons, these should be considered as separate blocks of same craton with different litho-structural attributes. Therefore, in this paper we consider EDC as the eastern part of DC. The gneiss, migmatite and associated rocks are lesser in volume in WDC. Whereas greenstone belts of EDC part are comparatively smaller in size than in WDC portion (Jayananda et al. 2013; 2019).

The schist-migmatite-gneiss complex cannot form at Earth's surface but at deeper part with fulfilment of required

pressure, temperature and other factors like fluid, differential stress etc. Hence the complex represents exhumed segment of the deeper continental crust and gives valuable insight into the processes of crustal genesis. These medium to high grade metamorphic rocks with distinguishable morphology like schistosity, crenulation, gneissosity, shear band, melanosome, leucosome (Fig. 2A–C) represent the different regime of deformation and onset of partial melting process. This led to variation in structures and associated deformation with increasing pressure and temperature related to time-dependant crustal growth mechanism.

So far, the specific field based structural attributes and the recognizable criteria of schist-gneiss-migmatite are not addressed in EDC part especially at outcrop scale. Most of

the works on tectonics were mostly done on the basis of LANDSAT image (Drury and Holt 1980; Chadwick et al. 2000; Chardon and Jayananda 2008; Jayananda et al. 2006). Categorization and characterization of gneisses and especially migmatite are not yet attempted systematically. The aim of this paper is to characterize and interpret genetic aspects of schist, gneiss, migmatite and granitoid based on structural attributes, which can give insights on crustal development mechanism.

Geologic setting

Geology of the Dharwar Craton is well known and there are extensive numbers of literature available (e.g., Swami Nath and Ramakrishnan 1981; Radhakrishna and Naqvi 1986; Naqvi and Rogers 1987; Chadwick et al. 2000, 2007; Chardon et al. 2008, 2011; Jayananda et al. 2006, 2015, 2018, 2020). The DC covering ~350,000 km² area is one of the major constituents cratonic nucleus in Peninsular India (Rogers 1986). This craton is bounded to the south by Proterozoic Southern Granulite Terrain (SGT), to the north by the Cretaceous Deccan Traps and the Bastar Craton, to the northeast by the 2.6 Ga Karimnagar Granulite belt and Godavari graben, to the east by the Eastern Ghats Mobile Belt and to the west by Arabian Sea. The EDC comprises mainly of greenschist to amphibolite facies greenstone belts of ~2.7 Ga age, along with felsic calc-alkaline plutonic, and volcanic rocks of ~2.7–~2.5 Ga age (e.g., Jayananda et al. 2000, 2013, 2020; Chardon et al. 2002, 2011; Dey et al. 2012, 2016; Manikyamba and Kerrich 2012; Manikyamba et al. 2017). Older (3.3–3.0 Ga) granitoids and metasedimentary rocks are rare in EDC and only present as remnants (Jayananda et al. 2000; Bidyananda et al. 2011; Maibam et al. 2011; Dey 2013). There are about 13 greenstone belts in EDC viz., Kolar, Veligallu, Kadiri, T. Sundupalle, Nellore, Ramagiri, Khustagi, Hutti, Sandur, Raichur-Mangalur, Garwal, Jonnagiri and Peddavuru (Jayananda et al. 2013; Goswami et al. 2016, 2017, 2019a, b). Amongst them, the southern greenstone belts are mostly N-S and the northern greenstone belts are NW–SE trending (Jayananda et al. 2013). The changes in this trend are possibly due to later deformation events during Eastern Ghats orogeny (equivalent to globally known Grenville orogeny), which is also responsible for crescentic shape of the Cuddapah basin.

Another important aspect is that the rocks are relatively younger in EDC than those in WDC (Jayananda et al. 2013). The Peninsular gneiss (~3 Ga) in WDC shows relatively older age than that in EDC (~2.8 Ga) in spite of their broad petrological similarities as TTG (Jayananda et al. 2020). Thus, the term 'Peninsular gneiss equivalent' is used in EDC. The EDC greenstone belts are dated 2.6–2.7 Ga and often intruded by the ~2.5 Ga potassic granitic bodies equivalent

to Closepet Granite. Different ages of Palaeoproterozoic dyke swarms are established with different orientation of stress field (French and Heaman 2010; Belica et al. 2014; Goswami et al. 2019a, b). The emplacement of younger granitic bodies in EDC exhibit linearity, parallel to the greenstone belts. Chadwick et al. (2000, 2007) designated them together as Dharwar Batholith to differentiate from Peninsular gneissic complex (PGC) of WDC. The EDC Basement Complex of Cuddapah and Bhima basins exhibit diverse nature. Weakly developed gneissosity and migmatitized remnants within younger granitoids are common. Patches of greenstone/schist belts and PGC equivalents nowhere cut across each other. Hence, it is difficult to establish chronological order on the basis of field observations. Mafic dyke swarms are the youngest lithounits in the basement (Soderlund et al. 2019).

The relationship between EDC and WDC is studied extensively in recent past (e.g., Gireesh et al. 2012; Dey 2013; Jayananda et al. 2018, 2020; Vijaya Rao et al. 2015; Bhaskar Rao et al. 2020; Jayananda et al. 2020 and references there in). As per the zircon U–Pb age and Hf isotope data interpretation of these earlier workers, two major juvenile crust accretion episodes involved depleted mantle sources at 3.45 to 3.17 Ga and 2.7 to 2.5 Ga. Crustal recycling was dominated during the intervening period. The Dharwar craton records clear evidence for the operation of modern style plate tectonics since ~2.7 Ga. Several schools of thoughts are available on tectonic models of DC. Considering most widely accepted views, it has been proposed that present configuration of DC suggest an exposed part of oblique cross section of continental crust due to a dominant northerly tilting by block faulting (Pichamuthu et al. 1981; Radhakrishna and Naqvi 1986; Rogers 1986; Newton 1990).

Field outcrop analysis

During the field work, different representative sectors (e.g., Wajhal-Hunasagi-Talikota area in north, Ramagiri-Penakacherla in central part and Rayachoti-Pincha-Bhakra-peta in southern part of EDC) were chosen to study the variation in deformation pattern (T1, T2 and T3 traverse in Fig. 1). Along with these, several number of transects were chosen throughout the area. In fact, all the litho-structural features visible in different outcrops were studied together to understand the structural fabric elements and their orientation, symmetry and relative ages, so that a sequence of deformation and intrusion events can be established.

The schist/greenstone belts have been metamorphosed to a lower grade compared to the gneisses/migmatites (Goswami et al. 2016, 2017, 2019a, b). However, well developed schistosity can also be observed in some younger granites and foliated gneisses, which comprise higher amount of



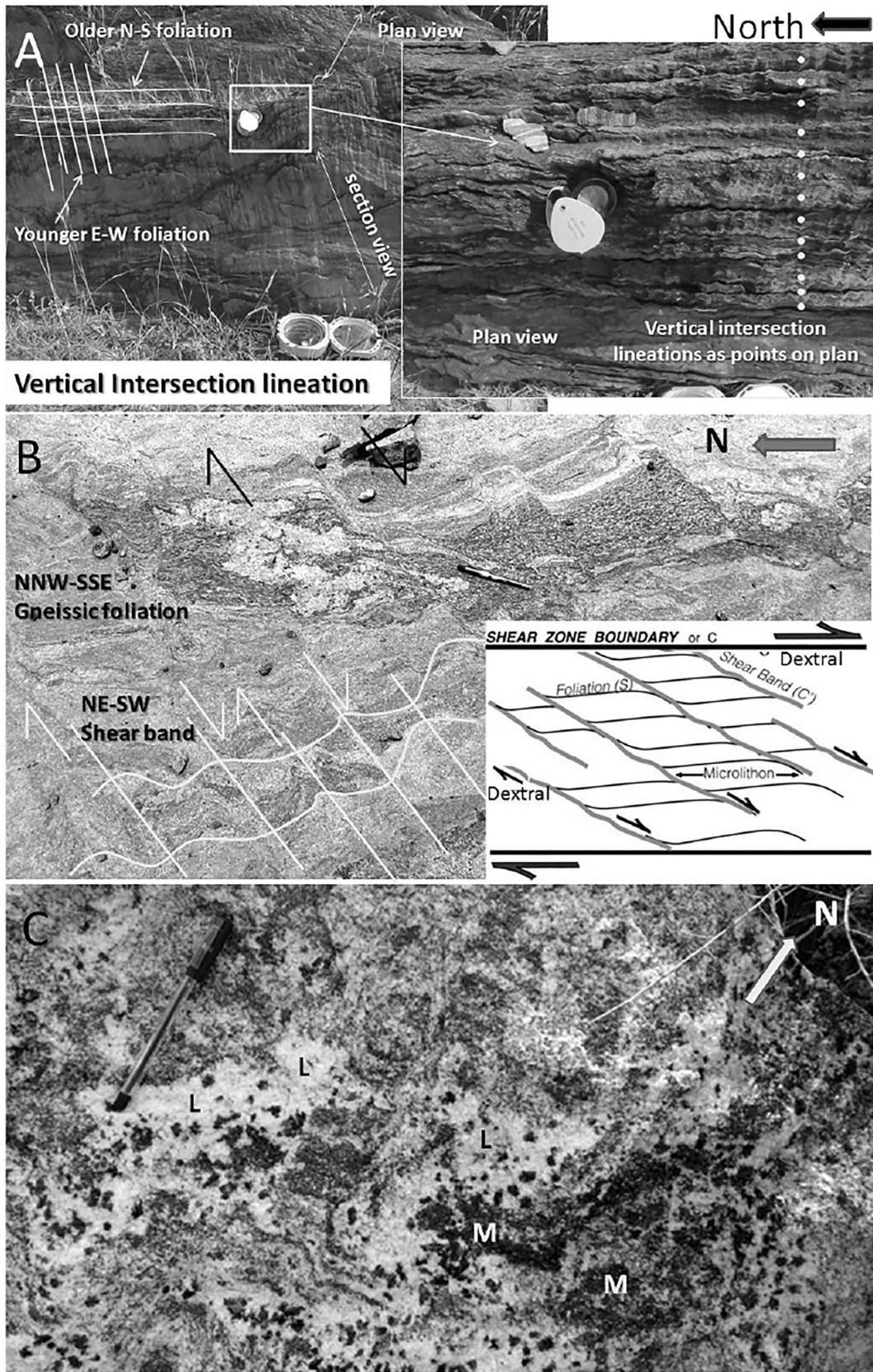


Fig. 2 A Outcrop photo of schist with crenulation (Ramagiri area, Anantapur dist. A.P., mesozone part). Vertical N–S and E–W foliation give vertical intersection lineation. B. Outcrop photo (plan view) of gneiss with dark–light banding (S of T. Sundupalle, Kadapa dist. A.P. catazone part). Dextral NNW–SSE shear zone boundary (C plane) is reconstructed with NE–SW shear band (C' plane) and micro-lithons form dark–light zones. C. Outcrop photo (plan view) of migmatite with patches of leucosome (L) and melanosomes (M) (S of T. Sundupalle, Kadapa dist. A.P. catazone part)

mica. The younger intrusive granitoids are not intensely metamorphosed and deformed as compared to foliated greenstones and gneisses except at places along their boundaries, where they are mylonitic. The lesser deformed areas with patches of greenstone belts indicate low strain zones, where the rocks survived intense deformation despite being older than gneiss-migmatite-granitoids.

The structural features are discussed according to the occurrences either in schist/greenstone belts or gneiss-migmatite and younger granite for better understanding of the influence of rheology (Table. 1). Then structural data base (Annexure 1, 2) is examined with reference to different deformation stages (i.e., time) and major occurrence location (i.e., if northern or central or southern part of EDC) of corresponding deformation fabrics (i.e., space). This study is helpful in demarcating the influence of combined factors like generation of different rock types vis-a-vis deformation events.

Structures in greenstone belts

Schistosity and shear zones are most common structural features in the greenstone belts. The original basaltic rocks in these belts are mostly metamorphosed in greenschist to amphibolite facies. Medium to coarse minerals with sheet or long prismatic grains (e.g., Biotite, chlorite, hornblende etc.) exhibit preferred orientation due to shearing during metamorphism and form schistosity. Broad pattern of deformation in the greenstone belts of EDC are mostly characterized by several phases of deformation and folding with different types of interference pattern and associated superposed folding (Figs. 3A–G and 4A–C). Mostly recumbent, upright, reclined folds and locally sheath folds are noted. The folds often show intrafolial nature with thinner limbs and wider hinges.

Throughout the greenstone belts, lithologic layering (S_0) is approximately parallel to primary metamorphic foliation (S_1), which is sub-horizontal in general. However, for initial planar fabrics S_0 (i.e., flow beds, volcanoclastic layers etc.) random arrangement of minerals and absence of any fabric is expected. Although S_0 do not show such primary features, there are no evidence of associated folding as well for developing S_1 . Therefore, S_0 and S_1 are not possible to differentiate from outcrop. Hence, it is naturally expected

to get initially developed recumbent folds (F_1) with horizontal axial planar foliation (S_1). This represents the first phase of deformation (D_1), with broadly horizontal axial planes, limbs (Fig. 3A) and ~E–W hinge line indicative of N–S shearing and associated effective compression vector acted sub-vertically. Clearly distinguishable and preserved fabric elements are more common after D_1 phase.

The horizontal axial planes of recumbent folds got refolded to upright fold (F_2) with NNW–SSE sub-vertical axial planar direction, during second phase of deformation (D_2) in response to E–W compression. Apparently normal stress on the plane was dominated during this event to develop upright geometry. Thus, the vertical to sub-vertical axial planes and cleavages are common along NNW–SSE to N–S direction. This upright folding of older recumbent fold often creates ambiguity near the older hinge areas which apparently give reclined geometry (Fig. 3A). Due to later developed shearing slightly plunging syncline and anticline are developed (Fig. 3F).

During the third phase of deformation (D_3), neutral folds (F_3) were developed with sidewise closure (Fig. 3B–D). The reclined nature of these neutral folds is notable from the ~90° pitch of axes on axial planes. This lead to develop sub-vertical S_3 planes at very low angle or often parallel to older S_2 due to shearing along N–S to NNW–SSE direction with effective compression at right angle (i.e., ~E–W). This also supports the tight to isoclinal nature of folding. During this episode plunging folds also appear locally near the preserved hinges of older fold and effects of later refolding, which complicated the outcrops further due to layer parallel shearing (D_4) and folding (F_4).

F_4 folds are not large-scale folds but locally superposed over F_2 and produce hook or flame like feature with NE–SW axial planar foliation (Fig. 4A, B) due to type 3 interference pattern (i.e., fold axes of older and later generation are parallel but axial planes are perpendicular. Ramsay 1967). Although shearing direction with respect to older fabric planes is same in case of F_3 and F_4 (i.e., broadly ranging from N–S to NNW–SSE), maximum compression (σ_1) and slip direction gets changed to right angle (i.e., E–W directed σ_1 in F_3 and NNW–SSE directed σ_1 in F_4). In these F_2 , F_3 , F_4 folds of D_2 , D_3 and D_4 deformation events respectively, the axial planes remain vertical to sub-vertical. D_1 , D_2 and D_3 events represent separate strain conditions as incremental strain. Subsequently, D_3 and D_4 is most probable product of progressive stress event, which often develop intrafolial folds.

However, foliation planes of second and third deformation events (S_2 and S_3) mainly controlled the regional outcrop pattern. The major F_1 recumbent folds are not well defined as compared to upright F_2 folds (which also exhibit reclined geometry of F_2 folds nearby the hinge areas of older F_1 folds). Minor local scale F_1 and especially F_2 folds are



Table 1 A comparative characteristics of Greenstone belt-Gneiss-migmatites and granulitoids of EDC

Properties of EDC rocks	Greenstone belt	Gneiss-migmatite	Younger granulitoid batholith
Age	~2.7 Ga (Jayananda et al. 2013)	~2.6 to 2.8 Ga and minor 3.1 Ga TTG (Jayananda et al. 2013)	~2.5 Ga (Jayananda et al. 2013)
Lithology	Meta gabbro, basalt, Chert, BIF, gray wacke	TTG and hornblende-biotite granite, anatectic product of older granite or metasedimentary protoliths	Alkali feldspar granite, granite, granodiorite, quartz syenite, syenite
Common deformation regime	Brittle-ductile in general	Ductile regime in general	Brittle regime in general
Major Structures	Tectonites, pillow breccia, crenulation fold, isoclinal fold, intrafolial fold, sheath fold, thin limb broad hinge fold, superposed fold, pinch and swell, boudinaged fold, mica fish, pressure shadow lineation, mylonite, brittle-ductile shear zone, S-C fabrics, different types of shear sense indicators, lit per lit intrusion and apophyses of granite, intersection lineation,	Sacchroidal and granoblastic structures, rootless fold, isoclinal folds, shear zone, ultra mylonite, S-C fabric, ductile shear zone, patch, dilatant, net and stromatic migmatites, schollen and raft, schlieren, folded migmatite, pygmatic fold, folded boudin, sheath fold, pressure shadow lineation, porphyroblast with different types of shear sense indicator, enclaves	Porphyroclastic, pegmatite vein layer, sheeted layers and conjugate and longitudinal joints, en echelon vein, pseudotachylite, proto mylonite, fault of different scale, fault breccia and gouge, augen structures of feldspar porphyry, feather joints, plumose structure, fibrous quartz vein, slickenside lineation, xenoliths
Degree of metamorphism and deformation	Low to medium grade greenschist-amphibolite facies metamorphism, schistose structures	Medium to high grade amphibolite to granulite facies metamorphism. Granulose and Gneissose structures	Very low grade zeolite-prehnite-pumpellite and contact metamorphism. ranging Cataclastic and Maculose structure

often observed in the meta-volcanics and BIF unit. After F_2 folding quartz veination along S_2 planes enhances the competence contrast to facilitate later generation folding and boudinage. The crenulation cleavage (S_4) developed by fourth phase of deformation (D_4) is variable in orientation but commonly intersects S_3 at angle of more than 45° . The steep (plunging $\sim 70^\circ$ – 80°) lineation locally developed on the schistosity plane is parallel to the axial plane of F_4 folds.

Foliation morphology varies from phyllitic and locally schistose in metapelites, to a spaced phyllitic cleavage in chloritic greenstone. Sheath folds are also observed with deformed outline and overprint of later superposed folding in the competent quartz veins due to its flowage capabilities (Fig. 4C). Such multiply deformed and tight to isoclinally folded greenstone units with lower metamorphic grade (greenschist facies) are often associated with interlayered high metamorphic grade gneiss (upper amphibolite facies) and migmatite. There are several places where relics of shearing related fold hinges are preserved. The most intensive and clearly visible F_3 and later developed folding (i.e., related to the NNW-SSE shearing), are often related to the contemporaneous development of localized secondary folds depending upon relative orientation with respect to shearing. However, layer parallel transposition with progressive stress events develops parallel schistosity planes (trending N-S to NNW-SSE) in greenstone belts and at certain places transposition process modified the older fold geometry.

Different types of lineation along with axial plane foliation are also noticed in greenstone belts. Pressure shadow/pressure fringe (Fig. 5A) with spindle shaped zones having aggregates of minerals formed on both sides of porphyroblasts/porphyroclasts is indicative of shadow zones that survived deformation and thus preferential settlement at these shadows. Mostly, NNW-SSE to N-S extension (σ_1 direction ranges from ENE-WSW to E-W) directions is manifested by such pressure shadow lineations. Reclined neutral isoclinally folded (D_3) veins are more common in the schist belt than upright isoclinal folds, which are related to later tectonics (D_5) of NNW-SSE normal stress and more prominent in southern part of EDC (Fig. 5B). During the D_4 stage horizontal quartz veins appeared along weak horizontal planes.

The haphazardly oriented quartz veins may be imagined as blanket, in which different parts exhibit different style of folding due to major component of localized stress vector. Therefore, the structural data of quartz veins are critically examined and carefully chosen before interpreting. In such cases other supportive data is also taken into consideration. Overall, the stages of folding in quartz veins can be understood broadly from the refolded sheath fold geometry (viz., Fig. 4C indicating three stages D_4 , D_5 and D_6). Another important feature is boudinaged folds, which indicate progressive regional sinistral shear along NNW-SSE direction. This event is linked to D_6 deformation when

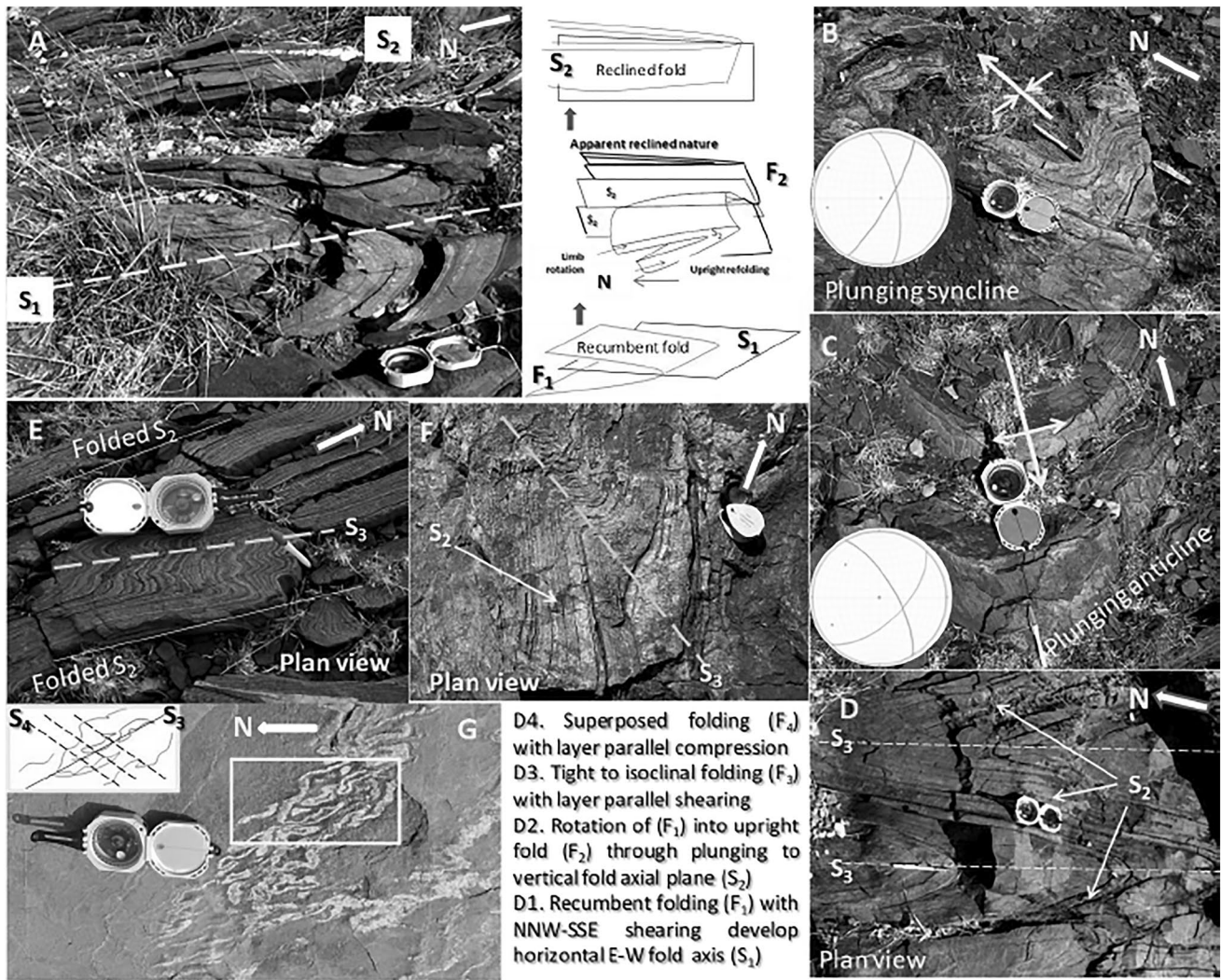


Fig. 3 A. Recumbent fold with horizontal fold axis and axial plane in schist belt. West of Ramagiri (mesozone part). Later imprints of folding is also manifested near rotated hinge portions. B. Northerly plunging syncline in schist belt with easterly dipping steep fold axial plane. ESE of Ramagiri (mesozone part). C. Southerly plunging anticline in schist. ESE of Ramagiri (mesozone part). D. Intrafolial neotectonic

fold with NNW sub-vertical axial planar foliation (S3). S of Ramagiri (mesozone part). E. Minor folding along with major isoclinal reclined folding in BIF layers. NNE of Ramagiri. F. NW vergence of open fold with in NNW trending BIF. G. Multiply folded schist belt near T. Sundupalle (catazone part)

transposition and transformation from extension to shortening field (and vice versa) are observed at different parts. Broadly the σ_1 direction for D_6 is found along ESE-WNW. Different segments are observed to define all the four major fields of shortening and extension (Fig. 5C and D). Initiation of granite generation was started after D_3 event, when quartz vein appeared as probable proxy of granitic magma at depth. However, profuse granite generation from anatexis of gneiss-migmatite is observed at southern catazone parts of EDC during D_3 unlike central mesozone and northern epizone parts of EDC. In the central mesozone and northern epizone parts younger granite is emplaced at least after D_6 . Tectonites suggest N-S to NNW-SSE direction of maximum stretching. Thus N-S to NNW-SSE horizontal stretching

lineations is common (Fig. 6A and B). However, the competent granitic layers with brittle signature of deformation implies D_7 event after granite generation and segregation along weak older foliation.

Development of boudinage imply the process of NNW stretching, necking and eventually segmentation of the layers (Fig. 6C). Pillow structures (Fig. 6D) are also used to measure the rotation from top–bottom determination criteria of pillow shape. The brecciation in pillow to become hyaloclastite is possibly linked to the D_2 deformation, which is also corroborating similarities of such rotation in other areas during upright refolding of older fabrics. Different degree of boudinage ranging from micro to macroscopic scale is exhibited by competent quartzo-feldspathic veins in



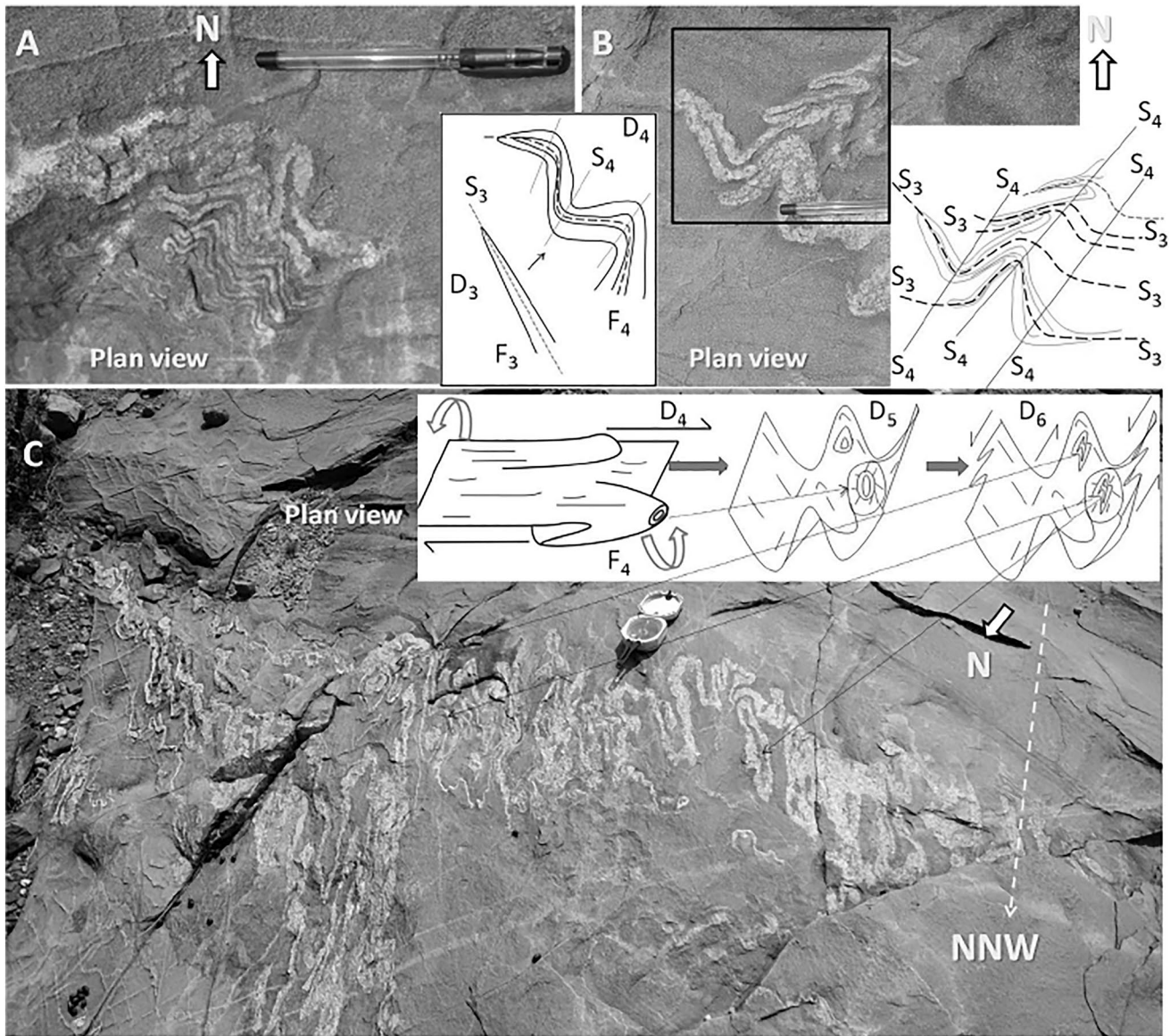


Fig. 4 A. Superposition of fold with type 3 interference in quartz ribbon/vein near T. Sundupalle (catazone part). B. Type threefold interference with flame shaped pattern in which phase 1 and phase 2 folds show parallel axes but perpendicular axial planes (Ramsay and Huber

1987). (T. Sundupalle west, catazone part) C. Outcrop plan showing refolding in sheath folds (T. Sundupalle—G Reddivaripalle area, catazone part)

schistose meta-basaltic hosts. The boudin axes are carefully observed and with reference to the axial direction boudin profiles are noted as symmetrical or asymmetrical. Mostly asymmetric boudinage give shear sense unlike symmetric boudins and pinch and swell structures, which are also common and associated with folding. They imply synchronous development in layers and veins of different orientation and significant competence contrast. Figure 7 shows a schematic 3D model of the few prominent phases of folding with associated foliation, lineation and boudin development stages (modified after Goscombe et al. 2004). The layer boundaries of the boudins are also of different types like convex,

tapering or straight (Figs. 5C and 6C). Asymmetric boudins are used for sense of shear determination because such boudins show lozenge shape and stretched at diagonally opposed corners (Fig. 8). The noncoaxial nature of strain with NW–SE trending dextral sense of shear are observed from such boudins.

Structures in gneiss-migmatite

Lit-par-lit intrusion mechanism can be described from the gneisses surrounding the greenstone belts, in the southern catazone parts (~broadly south of 14°N latitude) where

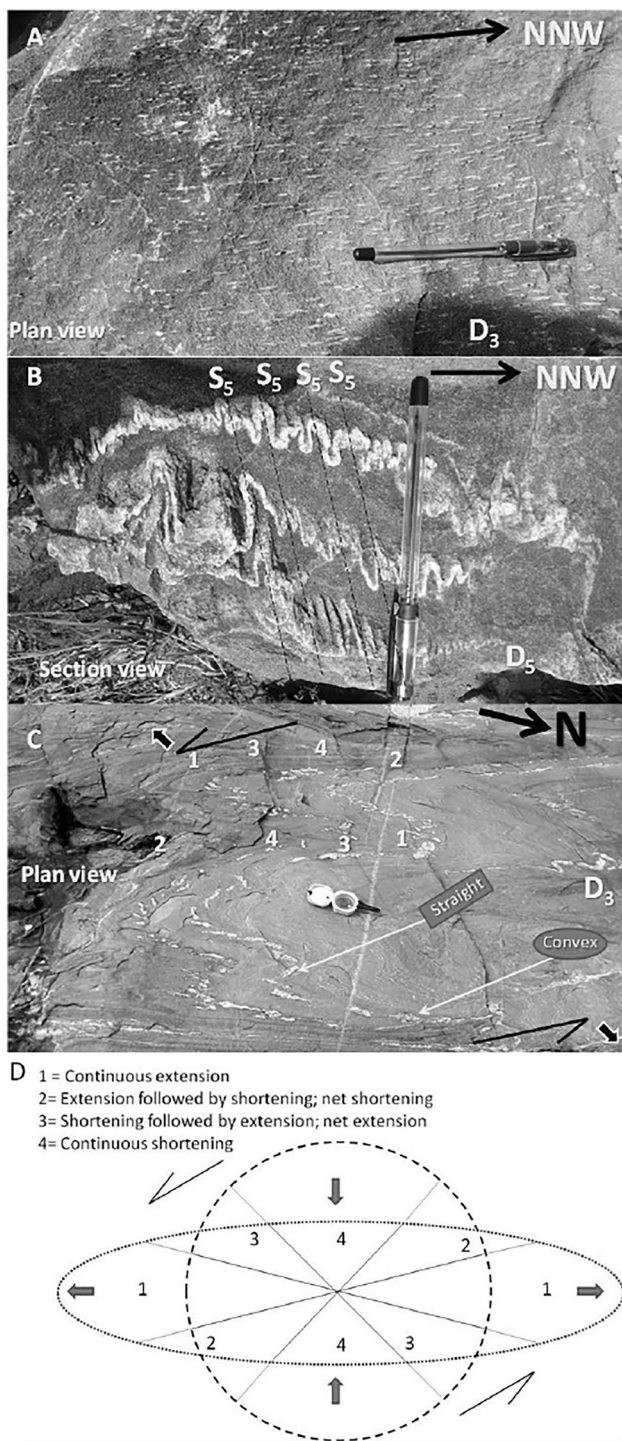


Fig. 5 **A** Pressure shadow lineation in schist belt metovolcanics (T. sundupalle west area, catazone part). **B** Isoclinal folding in quartz vein show upright nature with thick hinge and thin limb with steeply dipping axial planes. (T. sundupalle west area, catazone part). **C** Boudinaged folds with convex and straight outline of competent quartz vein. Boudin and fold association indicate competence contrast between meta volcanic matrix and quartz vein. Different domain of active stress component can be visualized from plan view (Brunton index to North). (Adavipalle area kadapa dist. A.P.). **D**. Strain ellipse for the boudinaged fold (Fig. 5C) indicates different domain of compression and extension field as marked numerically (Adavipalle area, catazone part)

granitoids and quartzo-feldspathic veins are observed to intrude along older schistosity planes (mostly S_2 and S_3) and develop alternating light and dark color bands (Fig. 9A, B). Broadly, majority of gneissic bands indicate about their origin from shearing associated layer transposition and pulling apart of layers (i.e., earlier folded layers, or compositional layers of different competence) during deformation event (D_4 and later). Therefore, all older features attend parallelism according to latest shearing, which results in the stretching of tight folds and separation of hinges from the limbs. The preserved rootless fold hinges often substantiated from this mechanism of NW–SE shearing (Fig. 9C) during D_4 . The medium to high grade metamorphic areas with gneisses and migmatites are often affected by younger granitic emplacements (D_6). Juvenile granite development is not a simple event but it comprises several long-lasting developmental stages.

Thus, to avoid ambiguity it must be noted in the field that deformation signatures within granite may or may not be preserved because at different depths along the craton characteristics of granite varies. However, it is quite natural that granite of deeper cratonic parts will have transitional nature with migmatite and often difficult to separate at places of anatexis. With subsequent segregation and upward emplacements, later stages of deformation may be imprinted at shallow level (i.e., epizone/mesozone parts). These areas (~ mostly south of $14^{\circ}N$ latitude) are characterized by the dominance of diatexites (anatexis of older rock to form neosome), especially leucosome and melanosome are very common. The light leucosome fractions show network channel with low dihedral angle ($\theta < 60^{\circ}$) between solid and melt phase (Vanderhaeghe 2009). This portion of migmatite can be considered as granite kitchen (Fig. 9D, E). The pre-partial-melting structures and paleosome are almost absent in such higher-grade metamorphic areas. Presence of migmatites suggests a temperature condition of about $650^{\circ}C$, in which the rocks begin to melt and produce such hybrid type rocks with both igneous and metamorphic characteristics (Sawyer 2008).

The gneissic layering is characterized by distinct colour bands due to alternating light quartz and/or feldspar-rich layers and dark biotite, amphibole rich layers. It is often observed that in some granite-gneiss-migmatite complex, feldspar grains are left behind due to its more rigid nature than quartz. Hence, quartz could flow as ribbon due to shearing but rigid feldspar remains either as laths or as oval eye-shaped (i.e., augen) grains (Fig. 9F). These are also called augen gneiss and mostly characterized as ortho-gneiss since they develop from anatexis of igneous protolith mostly granitoids and metovolcanics.

Low degree of anatexis is indicated by patchy metatexites and recrystallization of leucocratic minerals without much transport was noticed. This is because the



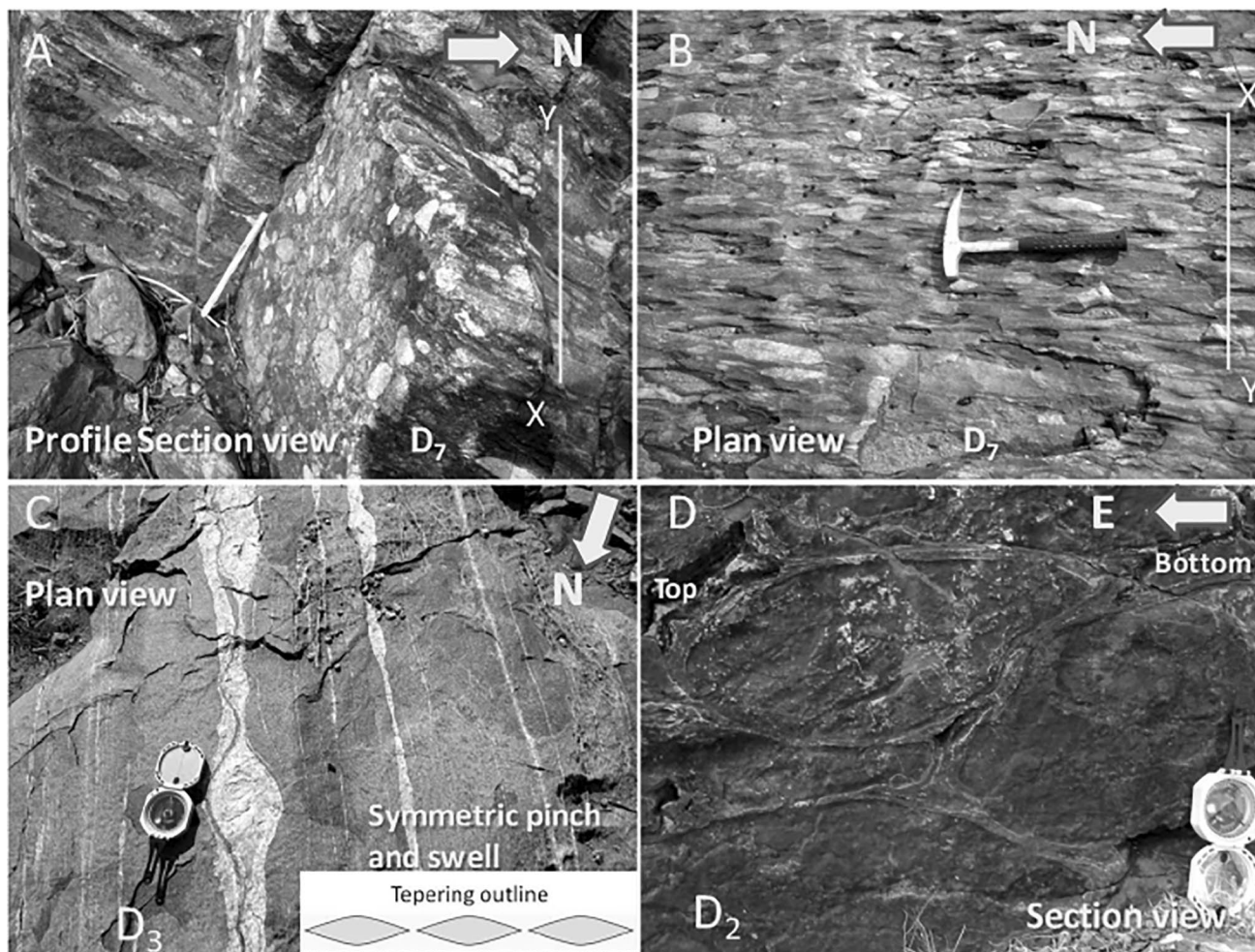


Fig. 6 A 3 dimensional outcrops of L-S tectonites developed in granitic veins intruded along schistosity of Kadiri greenstone belt (Dorigallu area, Anantapur dist. A.P., mesozone-catazone transition). B. Plan view of L-S tectonites showing elliptical stretched granitic fragments along N-S. (Dorigallu area, Anantapur dist. A.P.). Ham-

mer kept along N-S. C. Symmetric pinch and swell and boudins with tapering outlines in greenstone belt metabasics (G Reddivaripalle area, Kadapa dist. A.P., catazone) Brunton index to North. D. Rotated pillow structures in meta basalts (N of Ramagiri area, Anantapur dist. A.P., mesozone)

ferromagnesian dark minerals have higher melting temperatures than lighter quartzo-feldspathic minerals. Thus, lighter fraction could flow with low order stress towards dilatant sites and preferentially arranged as banding. Different morphology of migmatites is indicative of different stages of partial melting and stress conditions (i.e., static or dynamic mode). The paleosome-dominated metatexites of four sub-types (viz, patch, dilatant, net and stromatic) were differentiated in field (Fig. 10). Apart from this schollen or raft and schlieren type diatexites with enriched neosome were also noticed (Fig. 11). The migmatite stage itself indicate a plastic regime in which slight deformation can play immense role in creating passage of melt and creation of opening by faulting and shearing can enhance partial melting by pressure release induce drop in melting point.

Therefore, to create profuse granite during D_6 stage in the southern catazone segment along with deeper high temperature zone (static mode), deformation (dynamic mode) also helped in segregating the granite. The typical gradational contact between granite and older hosts in the southern extreme indicate higher temperature condition but low temperature contrast unlike the northern part with sharp intrusive contacts (epizone), where shallow crustal regime exhibited low temperature condition but higher contrast between emplaced hot granite with cooler country rocks.

Structures in younger granitoids

The younger late Archaean granitoids of EDC are mostly characterized by brittle and to some extent brittle-ductile regime structures. As such, absence of older ductile

Fig. 7 A. Block diagram showing the disposition most commonly observed features of vertical axial planar foliation, crenulation, stretching and intersection lineation in greenstone belts in field. B. A zoomed in plan view to reveal the imprint of later phase deformation signatures like isoclinal folding and boudinage and rotation by transposition (modified after Goscombe et al. 2004)

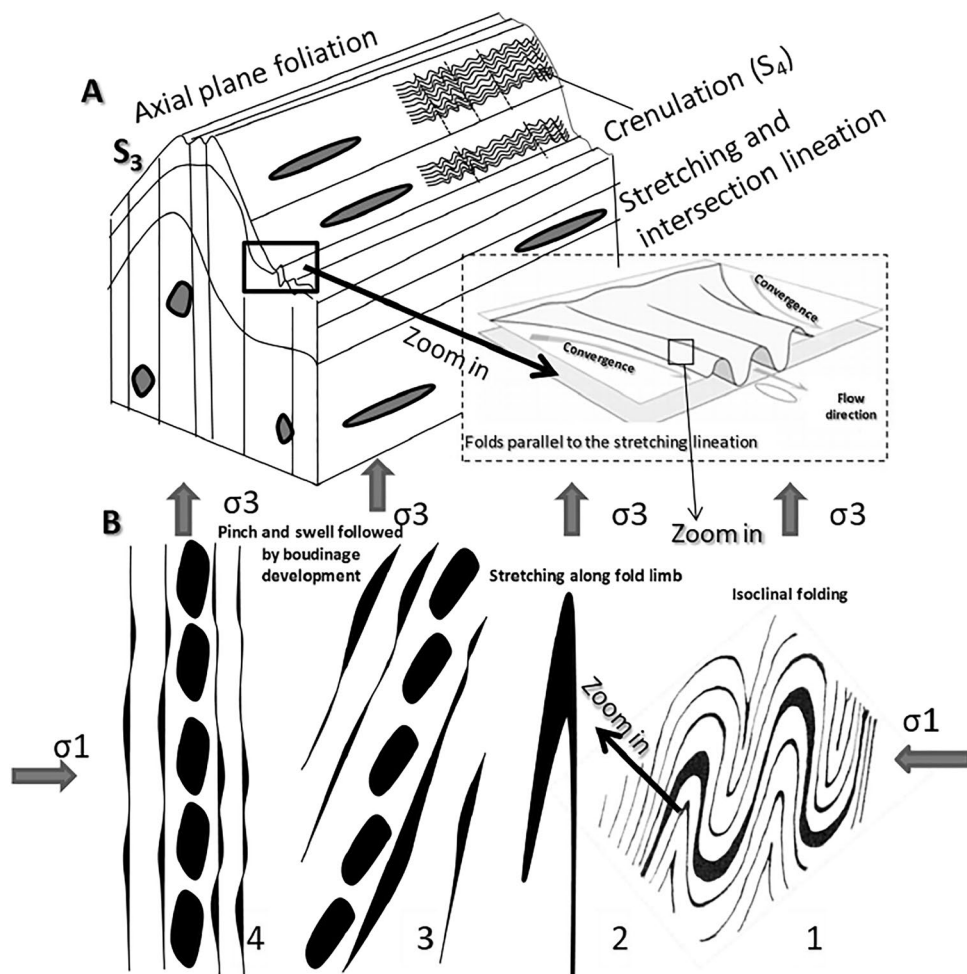
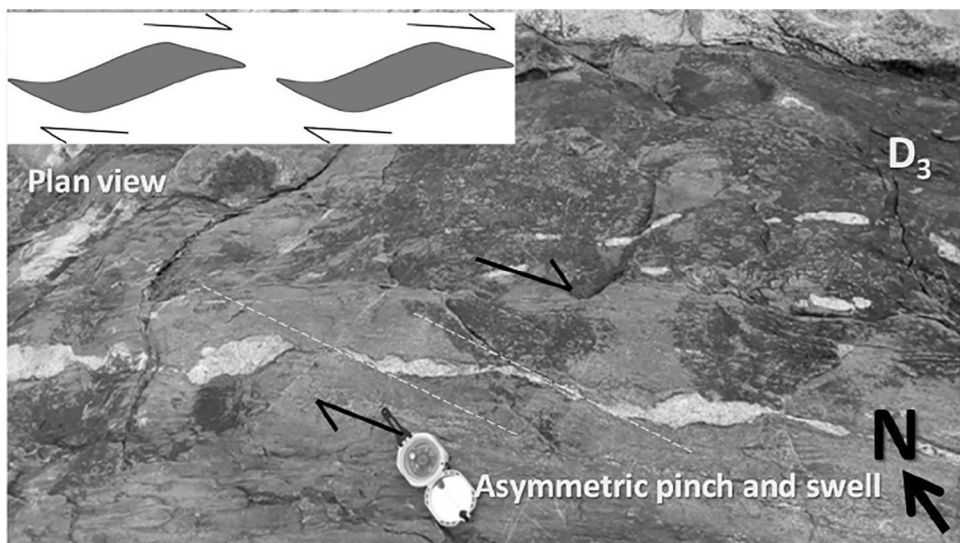


Fig. 8 Asymmetric style of pinch-swell and boudins in competent quartz vein surrounded by incompetent matrix of metabasalts. This is used as NNW dextral shear sense indicator (Brunton index to North). (Adivipalle area, Kadapa dist. A.P., catazone part)



deformation fabrics (D₁ to D₅) indicates crystallization and solidification of granitic magma took place after these deformation events. However, that does not mean granite melt generation, segregation and emplacement after these

deformations. There are evidences of syn-tectonic nature (Chadwick et al. 2000; Moyen et al. 2003; Jayananda et al. 2020) and most of the features are better observed under microscope. However, during D₅ stage of deformation



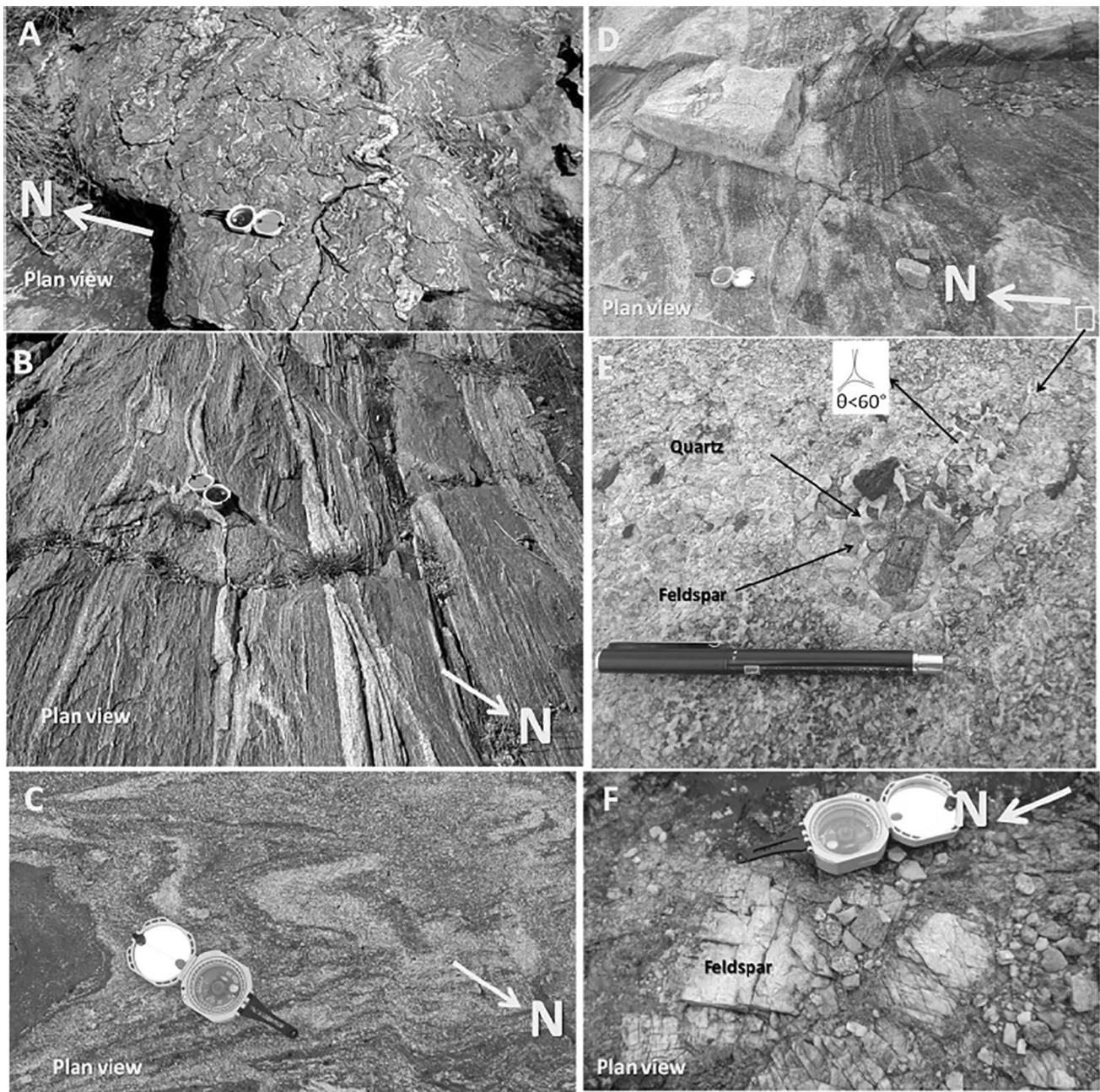


Fig. 9 **A** Lit per lit folded gneiss developed by quartzo-feldspathic intrusion along foliation in metabasalt. Later developed folds are visible with NNW vergence (D6). **B** Lit per lit intrusion of younger granitoid veins along foliation planes (S2 and S3) in greenstone belts. **C** Gneiss with isoclinal rootless fold hinge segments (F3) remaining with colour banding due to layer parallel transposition. **D** Low degree anatectic and associated quartz ribbon development in gneiss-migmatite. Linear bands developed due to preferential alignment of leuco-

some flow. **E** Close view of small part of static mode migmatite, in which feldspar remain intact and quartz start flowing around feldspar. Considering quartz as leucosome melt the low dihedral angle can be found to substantiate material flow with melt channel development. **F** Feldspar crystals left behind after quartz removal (Reddivaripalle-Adivipalle-Madithadu areas, Kadapa dist. A.P., catazone segment) (Brunton index and pen cap oriented to North)

intense migmatite and diatexitic fractions started appearing in the southern parts. Further, D_6 fabrics also frequently observed to develop pathway for anatectic melt segregation in the form of tube-like channel defined by transposed linear fabrics. Therefore, D_5 can be linked with generation and D_6

with segregation and transport of granitic melt. Therefore, after D_6 granite emplacement, cooling and solidification occur. Thus, the granite outcrop does not show any pre D_6 ductile features as such. The newly generated granitic melt got well defined pathways along older foliation planes to

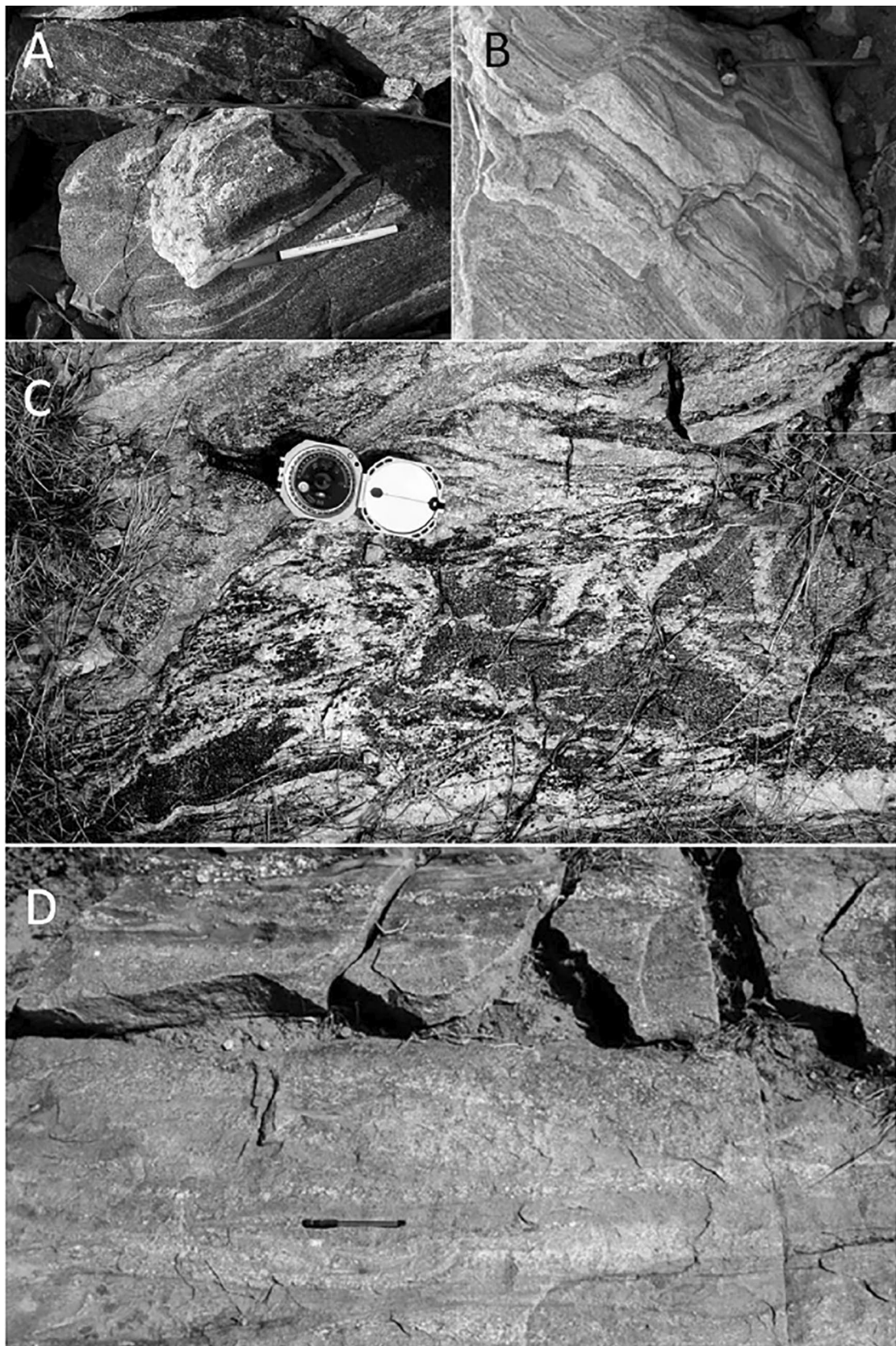


Fig. 10 Different types of metatextitic migmatites. **A** Patch. **B** Dilatant. **C** Net structured. **D** Stromatic types (pen cap to the north, hammer head to the north, brunton index pointing north). (Ramagiri, Reddivaripalle-Adivipalle area, Anantapur and Kadapa dist. A.P., catazone part)



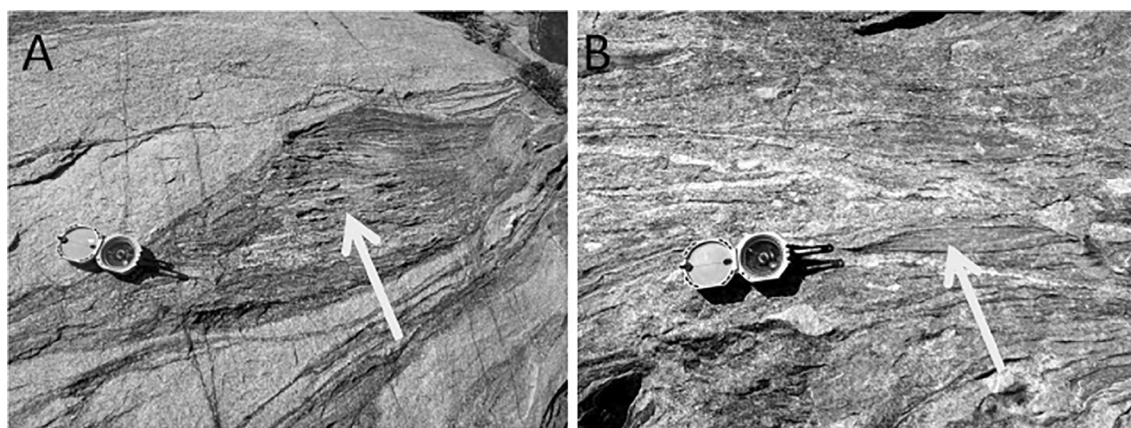


Fig. 11 Two types of diatexitic features in migmatite marked by arrow. A. schlieren. B. schollen and raft structures (brunton index pointing north). (Reddivaripalle-Adivipalle area, Kadapa dist. A.P. catazone part)

exhibit lit-per-lit intrusions, which is later affected by brittle-ductile deformation to form tectonites (D_7). Generally, the younger granite occurs as distinct hillocks of composite/simple plutons. Near northernmost part of EDC, along the Bhima basin margin, pink alkali feldspar granite with megacrysts of K-feldspar are exposed with sharp discordant contacts with older rocks. While, the southern part of EDC along the Pincha-Bhakrapeta (south of Cuddapah basin) tract is characterized by diatexitic granite with gradational patchy contacts with older rocks. The intensity of ductile deformation features, migmatites and gneisses increase toward south.

Development of protomylonite and mylonite indicate a ductile to brittle-ductile transition regime in the central block (Fig. 12A, B). The shear bands with S, C and C' planes indicate progressive shearing and mylonitization. The incompetent rocks like biotite rich schist and gneiss commonly display more ductile behavior than quartz and feldspar rich granitoids with higher competency. The brittle structures like veins and dykes are often sheared and reactivated in granite. The pseudotachylite is formed due to shearing and associated heating during brittle fracturing. Few outcrop sections show horizontal quartz vein and high angle reverse faults, indicating unloading and exhumation (Fig. 12C). Quartz veins often show shearing with en-echelon pattern. Mica rich granite often developed schistosity due to parallel alignment of sheet silicates.

Overall, the granitoids represent sheet like bodies with slab by layerings formed due to exhumation. There are few outcrops exhibit dextral shearing with marked displacements of older fracture as well as pull apart depression cracks development (Fig. 12D). There are no discrete contacts between granite and anatexis product in the southern part of EDC, where granite show catazone character (Fig. 12E). Close observation of such granite reveals melting of quartz around feldspar crystals, which gives idea on diatexitic

granite (Fig. 12F). At certain places dextral bookshelf tectonics can be interpreted from shear zone (Fig. 12G, H). Since the southern part represents deeper crustal segment association of such shear zones and migmatites-gneiss are more with granite. In this southern part granite is possibly generated as diatexite and the segregated upward (i.e., northerly in present day). Thus, segregation and migration features (e.g., apophyses, contact metamorphic zones) are more towards north. Extreme northern sector is characterised by relatively static emplacement features (e.g., K-feldspar megacrysts, sharp contacts with country rocks) of shallow epizone.

Use of principle of inclusion and cross cutting relationship

After a detailed observation and analysis of acquired data from the entire study area, sequence of established deformation from each outcrop are combined to build up a representative standard sequence of deformation events. Based on the principle of intrusive relationships using cross-cutting contacts, granite is found to be younger than greenstone and gneiss. Mafic dykes, quartz and pegmatite veins are further younger to granite. It is obvious that shear zones and faults affecting a particular lithounit must be a later event than the formation of that lithounit itself. With this analogy, different episodes of ductile shearing were interpreted as pre, syn and post granitic in time. The faulting events are mostly later shallow brittle phenomenon after granitic emplacement.

The principle of inclusions and components are also used in field to understand that inclusions must be older than the host that contains them. Hence, xenoliths of mafic supracrustals within gneiss and xenoliths of greenstone and gneiss within granitoids explain the sequence of rock formation. In fact, several episodes of greenstone & TTG

gneiss and then granite appeared in EDC which can also be reaffirmed by absolute dating. In fact, radiometric age data (Zircon U–Pb) from other parts of EDC showed ages of TTG (~3.36–2.96 Ga), greenstone (~2.74–2.70 Ga), gneiss (~2.67–2.60 Ga) and younger felsic plutonic and less common felsic volcanic rocks (~2.57–2.52 Ga) (Jayananda et al. 2020).

The contacts of the schist belts with the granitoids are typically intrusive, but are tectonic also at places (Fig. 13A, B). Granitoids mostly intruded metavolcanics near greenstone belt margins. The lit-par-lit intrusion along schistosity planes, apophyses and intertonguing relationships and effects of rare contact metamorphism are common around the margins of many granitic plutons (Fig. 13C, D) and these suggest later development of juvenile granite plutons. Contact metamorphism with chilled margin (aureole) and apophyses are more especially in the northern and central sector of EDC. This implies temperature contrast between granite and country rocks are higher than that in the southern part. Granite tongues are often extended from main body to the greenstone belts, where competence contrast led to development of pygmy folds (Fig. 13E). This indicates that later formed granite intruded over greenstone and then shearing associated deformation took place. The xenoliths of greenstone patches with preserved shear sense indicator (σ) within granite also supports the similar sequence of events (Fig. 13F).

The generalized methods applied throughout the terrane to determine shear sense are to use the rotation/displacement of marker features such as mafic dykes, quartzo-feldspathic veins, xenoliths and banding over the shear zones. Altogether, the combined observation suggest that ductile shearing is more common before granite intrusion and thus older supracrustals exhibit more ductile features than later granite, which mostly show brittle-ductile to pure brittle shear associated deformation. Therefore, granite segregation can be related to a contemporaneous exhumation from ductile to brittle-ductile regime.

Petrography

The granoblastic polygonal texture in gneiss and irregular grain boundaries in metavolcanics of greenstone belts suggest higher and lower metamorphic grades respectively. This is due to grain boundary migration towards a low-energy configuration since shorter and straight boundaries need lower free energy than irregular ones (Fig. 14A), also known as grain boundary area reduction (GBAR) (Vernon 1983, 2004; Poirier 1985; Passchier and Trouw 2005). To be more precise greenstone belt rocks indicate high temperature grain boundary migration (GBM) with low flow stress (Passchier and Trouw 2005). The granoblastic

fabrics indicate relatively fast diffusion and recrystallisation which lead to generation of melt pockets along grain boundaries (Urai et al. 1986). Such grain scale deformation is repaired by grain boundary area reduction and formation of gneiss. Although strong macroscopic/mesoscopic deformation features like isoclinal folding is present in gneiss (Fig. 14B), small scale granoblastic fabrics indicate apparently undeformed gneiss. The brittle deformation is manifested by fractures across and between grains and the resulting fragments is found to move relative to each other. Microstructures indicative of cataclastic flow include micro-fractures and displacements of cleavage as well as displacement and rotation of rigid particles (Fig. 14C).

Different events of the P–T–t history are preserved in different part of the terrain. Poikiloblastic textures as ortho pyroxene inclusions in clino pyroxene (Fig. 14D) indicate prograde metamorphism. Hydration reactions are evidenced by replacement of anhydrous mineral (e.g., ortho pyroxenes) by hydrous minerals (amphibole and chlorite), during retrogradation with exhumation (Fig. 14E, F) which led to form such outcrops to be exposed to the surface. The epizone segments in the northern part often characterized by different types of symplectites, fine grained intergrown crystals of quartz and plagioclase and alkali feldspar. Thus, metamorphic assemblage indicates about clockwise P–T–t path. Further justification of the P–T–t path is substantiated in discussion part. Grain-scale fracturing (i.e., a mechanism of removing fluids) connotes about the fact that during prograde metamorphism possibly devolatilization reactions took place. However, in normal scale it does not show any microstructural evidences. Retrograde metamorphic imprints do not show complete changes in mineralogy of earlier prograde event due to the fact that chemical reactions run faster at higher temperature. Moreover, removal of fluids during devolatilization caused scarcity of available fluids.

However, this is a qualitative study in which mineral content and textural aspects from rocks at different localities suggest preserved portions of different parts of a pressure–temperature–time path. However, exact quantification should be possible after quantitative studies like thermobarometry and pseudo section study.

The most commonly observed hydration reaction suggests a later destruction of previous prograde features possibly due to textural and chemical re-equilibration of the rock during retrogradation. Moreover, the lower diffusion rate for low temperature retrograde condition, the mineral composition of the terrain mainly reflects a specific part of the total P–T path following peak metamorphic conditions. Brittle fracturing of older plagioclase indicates shallow depth (Fig. 14G) and subsequent quartz vein development is signifies later unloading related to fracturing (Fig. 14H).



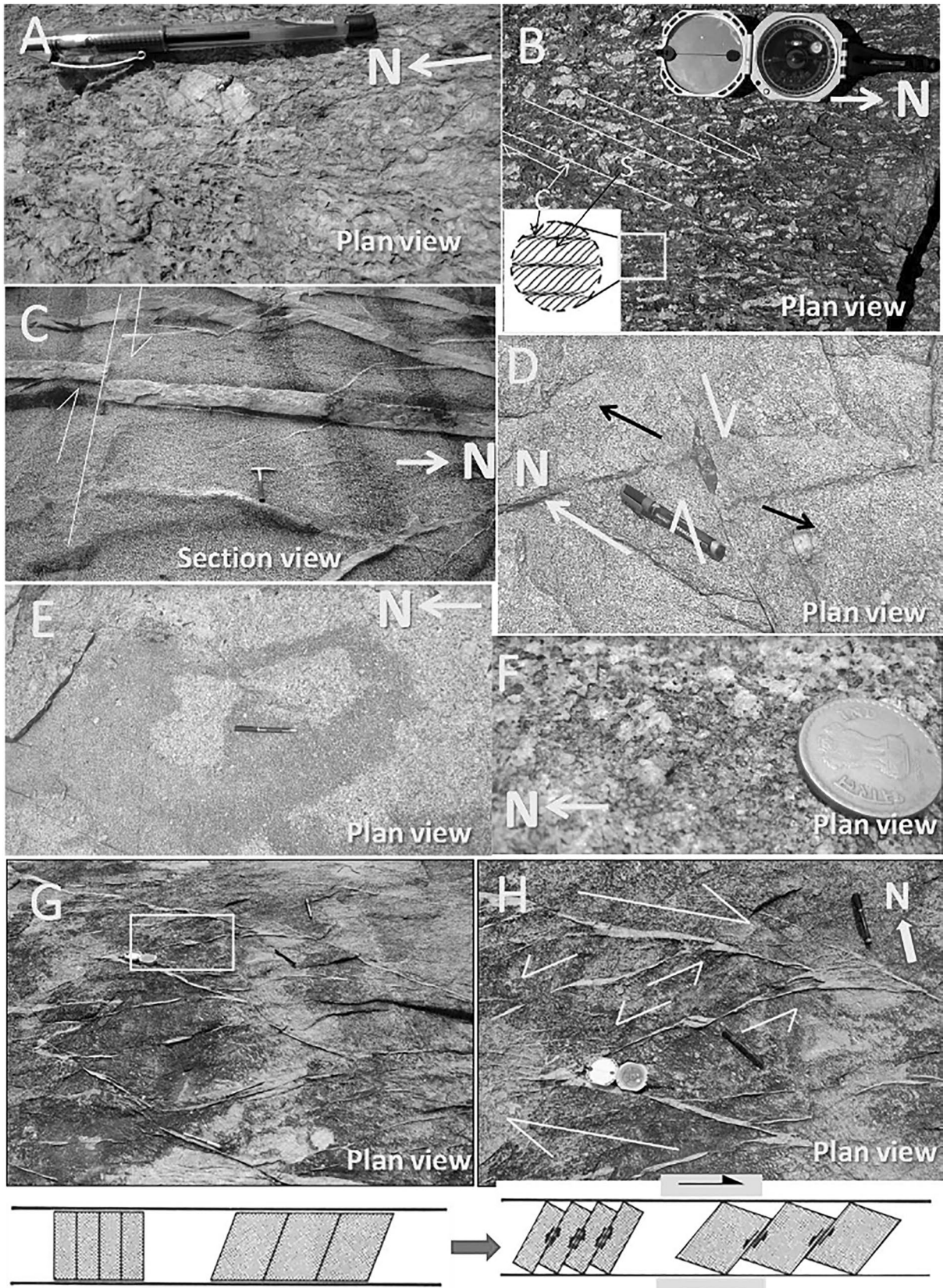


Fig. 12 Different brittle and brittle-ductile regime deformation features in younger granitoids. **A** mylonites with quartz ribbon around feldspar. T. Sundupalle, catazone segment. **B** S-C proto mylonites. Ramagiri, mesozone. **C** Quartzo-feldspathic veins and small scale faulting in younger granite. Dorigallu ghat section, mesozone-catazone transition. **D** Dextral strike slip faulting and pull apart basin structure in granite. Pincha area, catazone part. **E** diatexitic granite and migmatite association. Pincha, catazone. **F** partial melting and quartz ribbon flow around feldspar crystals, catazone. **G** shear zone with bookshelf feature of blocks rotation in response to dextral shear, catazone. **H** zoomed in view for better illustration. (Santhigettu area, Kadapa dist. A.P.)

By synthesizing all the above discussed macro and micro structural as well as textural evidences collected from both the high- and low-gradeterrains it can be concluded that there was a deeper ductile regime which gradually exhumed through brittle-ductile transition to brittle surficial condition during northerly crustal tilting with block faulting (evidenced by increasing grade of metamorphism from greenschist to amphibolite towards south and progressive transition from epizone through mesozone to catazone

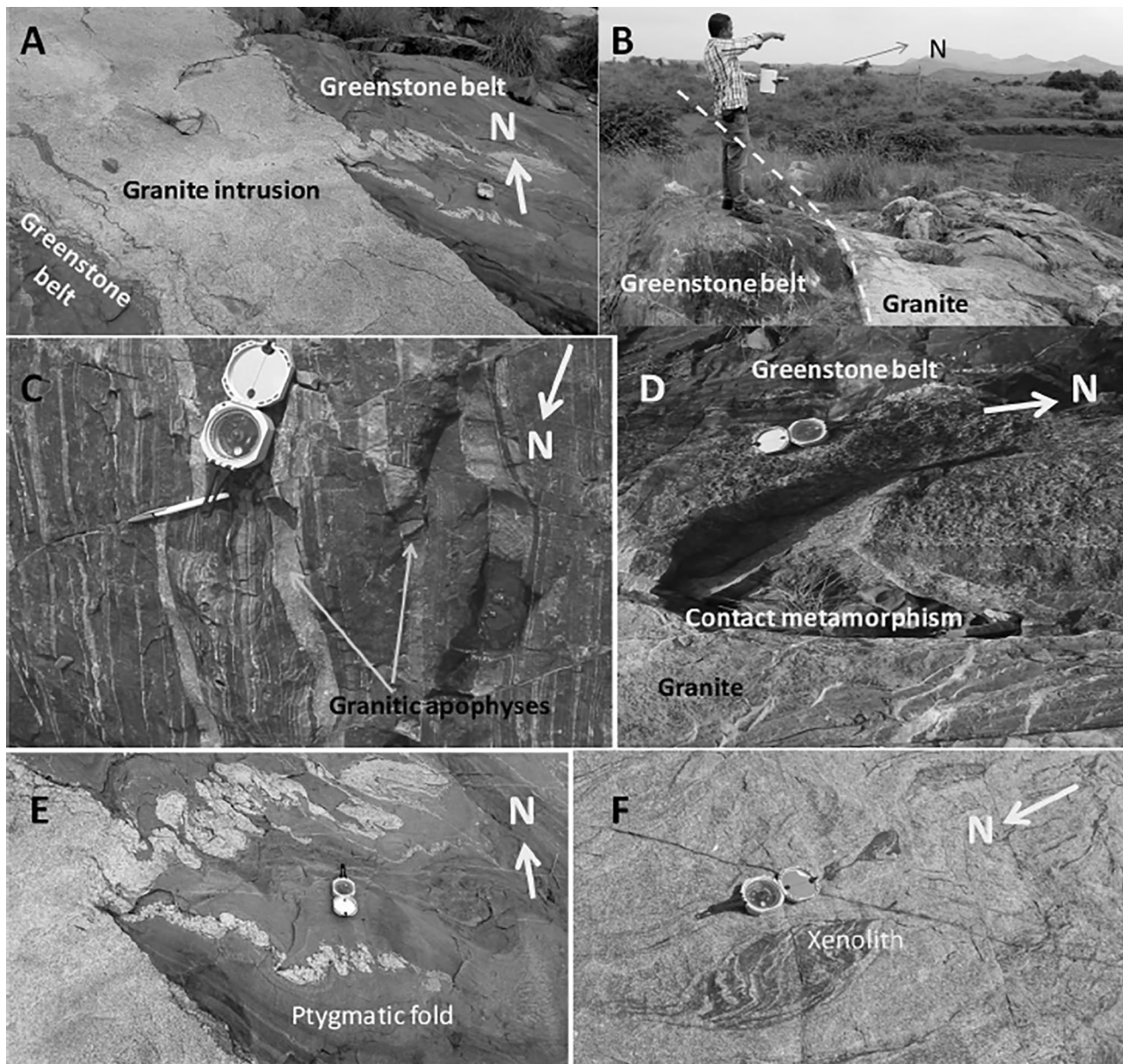


Fig. 13 **A** Emplacement of coarse granite along foliation in greenstone belt indicating intrusive contact zone (D6), catazone segment. **B** Presence of fault along the granite-greenstone contact indicate tectonic contact, catazone. **C** Apophyses of granite indicate later intrusion and small scale displacement of apophyses indicate later phase tectonism, mesozone. **D** Contact metamorphism along granite-green-

stone contact, mesozone. **E** Granite tongue extended into the greenstone belt and later deformation led to development of folds, mesozone. **F** Meta basalt xenoliths of greenstone belt in sheared granite, catazone. (Ramagiri-Pennakacherla, Reddivaripalle-Adivipalle area, Anantapur and Kadapa dist. A. P.)



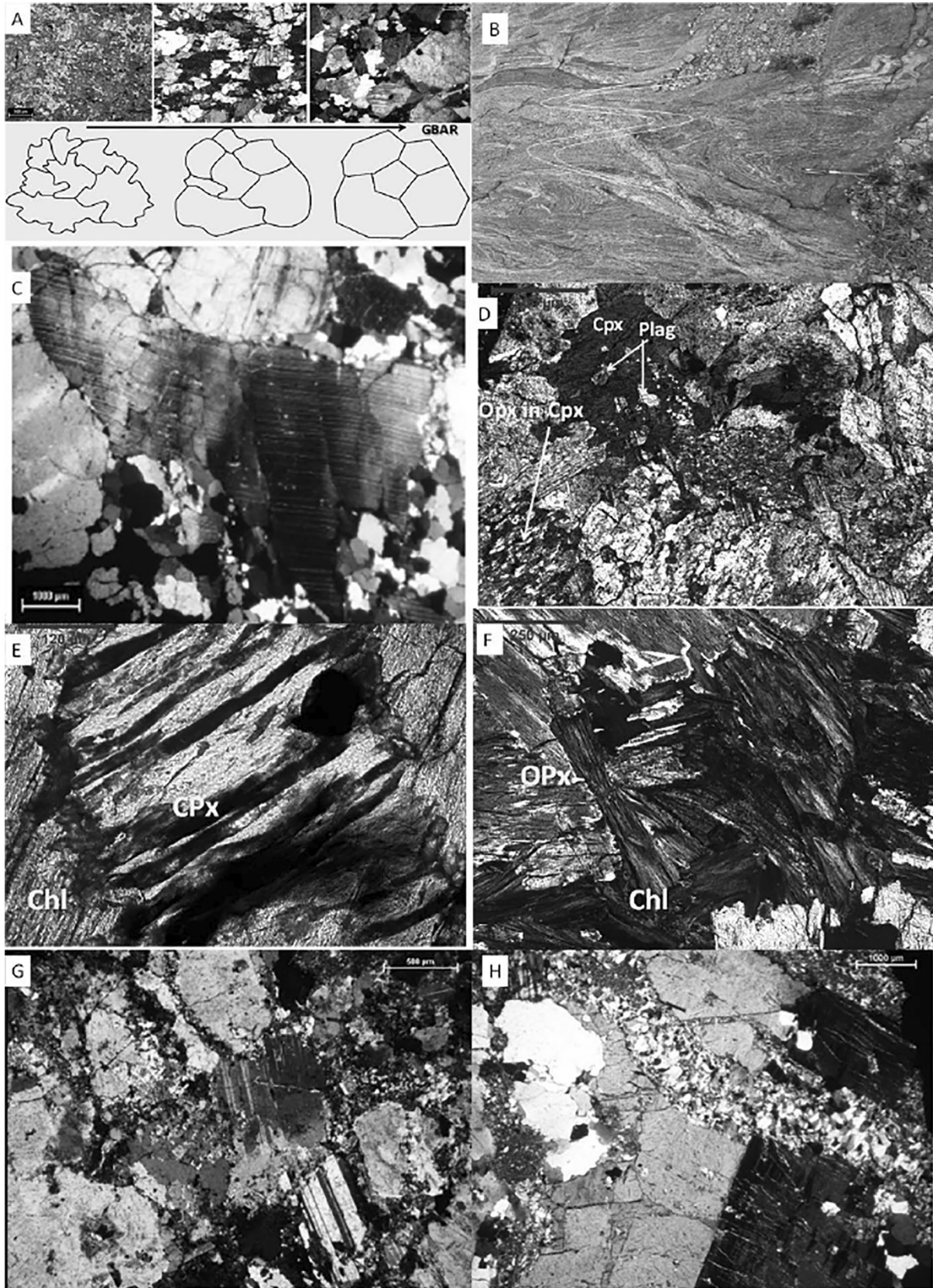


Fig. 14 **A** Photo micrographs and sketches showing petrographic difference between lower grade schistose rocks and higher-grade gneissic rocks and process of grain boundary area reduction (GBAR, inset after Passchier and Trouw 2005). Mangalur and T. Sundupalle schist belt and granitoids. **B** Isoclinal fold in gneiss (F3 and D3). Adivipalle, catazone. **C** Microstructure indicate cataclastic flow, displaced twin lamellae with kinked plagioclase feldspar TL, XN. Hunasagi.epizone part. **D** Ophitic texture between clino pyroxene (Cpx) and plagioclase (Plag) and poikilitic texture between ortho pyroxene (Opx) and Cpx, mesozone part. Ramagiri schist belt. **E** Cpx altered to chlorite (Chl), mesozone, Ramagiri schist belt. **F** Opx altered to Chl indicate hydration. Mesozone, Ramagiri schist belt. **G** Brittle fracturing in plagioclase grains of younger granitoids. Wajhal (epizone segment). **H** Quartz vein and fracturing in younger granitoids, Wajhal (epizone segment)

from north to south implies exposed deeper crustal segments towards south). Evidences of tectonic events are observed from overprinting of deformation fabrics. These are also substantiated from field observation on post granite unloading and exhumation features.

In this work, minutely observed features are noted down one by one. In fact, with increasing degree of anatexis the rock property or especially rheology also automatically gets changed and hence slight stress can be enough to transpose fabrics when anatexis continue. Actually, the event sequence is Metamorphism-crustal melting (partial & phase wise)-slight stress related channel creation-melt segregation-ascent and emplacement at shallow level as magmatism.

Discussion

The metamorphic grades in EDC varies from low to high depending up on the terrain like greenstone, gneiss-migmatite and granitoids because metamorphic changes in mineralogy, grain size, shape, and chemical composition dependent up on protoliths of different rheology. It is a fact that greenschist/amphibolite facies metamorphism cannot occur at the Earth's surface but at certain depth range with optimum pressure (P) and temperature (T) and time (t). Since we are getting metamorphic rocks of greenstone belt (volcano-sedimentary assemblages), a qualitative understanding can be drawn that some prograde path in P–T space caused burial and metamorphism followed exhumation back to the surface along a retrograde path. After integrating published P–T data to visualize quantitative aspects (Jayananda et al.

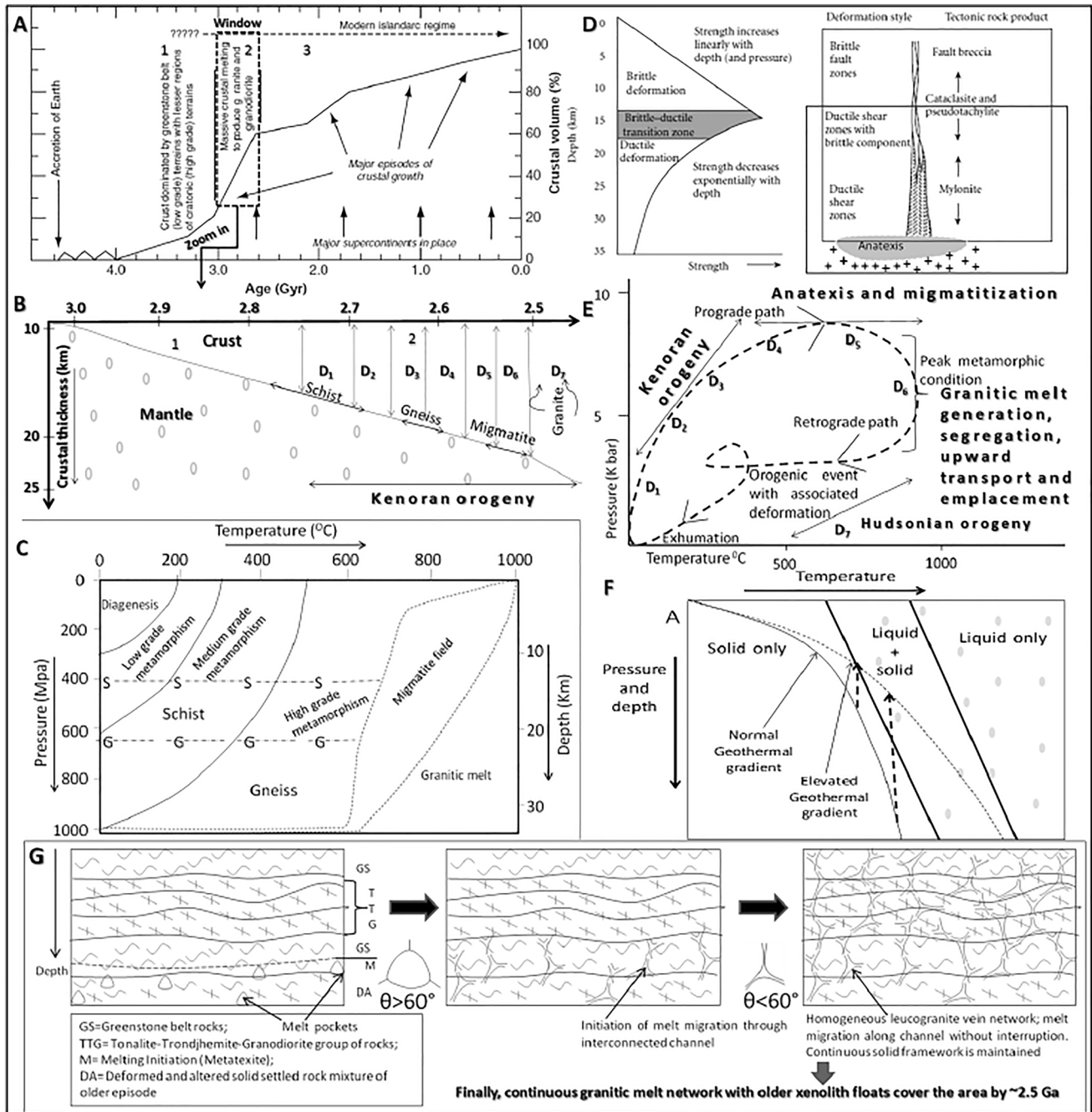
2011, 2013; Peucat et al. 2013), it is found that DC exhibit a systematic increase in P–T conditions from north (400 MPa–450°C) to south (800 MPa–800°C).

It is also visualized that the P–T path can be either clockwise or anticlockwise. Now the point is how to examine such path so that we can have ideas on burial and exhumation process? Our field-based studies with supportive microscopic examination of petro-mineralogy and texture give ideas on qualitative aspects. However quantitative studies like radiometric dating and thermodynamic modeling can provide further information, which is beyond the scope of the present paper context.

The present context deals with the Archaean deformation and metamorphic history of EDC. The time relationships among greenstone, gneiss-migmatites and granitoids with their corresponding structural and metamorphic attributes reveal the tectonic history of EDC. Apart from rheology, the development of schistosity, gneissosity, migmatites and granitoid magma can be linked to the progressive increase in the pressure/depth and temperature with time. Therefore, the progressive increase in the grade of such regional and burial metamorphism can be related to crustal growth with time. However, granitic intrusions in the upper crust cannot be considered as addition to older crust because these are derived from anatexis of older deeper crustal differentiates. This observation is supporting the earlier view of Taylor and McLennan (1981, 2009) and as per their standard crustal evolution model major episodic pulses of crustal growth is most acceptable than steady-state model.

In the EDC rocks of older TTG (~3.36–2.96 Ga) are rare and most of the meta basics of greenstone belt (~2.74–2.70 Ga), gneiss (~2.67–2.60 Ga) and younger felsic plutonic and felsic volcanic rocks (~2.57–2.52 Ga) (Jayananda et al. 2013, 2020) occupy over 99% area. Thus, present structural data implies geological attributes of particular time window (Fig. 15A), during which initiation of older crustal melting started with enhanced rate of crustal growth in terms of newly added lighter granodioritic gneiss and granite at the end. Therefore, net volume enhancement with time due to increasing lighter fraction in the upper crust caused change in geothermal gradient. Older rarely observed supracrustal rocks of greenstone-TTG association is falling in the field 1 and presently studied data, i.e., commonly found in field indicate field 2 in the modified growth rate curve of the continental crust (Fig. 15A). The story of





field 1 in crustal evolution curve (Fig. 15A) suggests that crustal thickness was less at the beginning and there was no support below the thin crust, because hot molten materials were more. When greenstone belt volcanism took place over initially build thin crust, they started sinking with cooling due to dense material content (rich in Fe–Mg rich minerals).

During the period of field 2 (Fig. 15A) significant accretion events occur. Thus, it is actually relevant in terms of major acceleration pulse of crustal growth due to Kenoran orogenic event (Goswami et al. 2019b) with associated ductile deformation stages.

Fig. 15 **A** Growth curve of continental crust (after Taylor and McLennan 2009), modified to show present window i.e., time range of EDC schist-gneiss-migmatite. Major fields (shown as 1, 2 and 3) shown to differentiate pre and post Kenoran orogeny events. **B** Enlarged representation of the window 2 to interpret the field data with reference to deformation stages and associated crustal growth vis-a-vis present litho-structural attributes. **C** Diagram showing temperature and pressure conditions of diagenesis, different grades of metamorphic conditions, and the high temperature magmatic field. (modified after Nelson 2018). **D** Diagram showing brittle-ductile transition within Earth and corresponding structural deformation features (modified after Duba 1990). **E** Estimated crustal thickness with reference to age are converted to depth/pressures data and corresponding temperature of standard anatexis melt generation data plot to define a P–T–t path (qualitative) of EDC with reference to deformation events. Three portions are interpreted from combined field and microscopic studies. Initial deformation and associated thickness enhancement of crust indicate prograde condition and Kenoran orogeny related deformation stages. Further thickening lead to anatexis, migmatite and initiation of granite melt generation. Subsequent segregation, transport and emplacement of granite followed by the retrograde path is related to exhumation, also substantiated by hydration of ortho pyroxene into chlorite, amphibole. Brittle deformation and fracturing of plagioclase and recrystallization and flow of quartz ribbon indicate deformation in brittle-ductile regime. Chloritization of all pyroxene is final dehydration during retrograde exhumation and transition to brittle regime along with Hudsonian orogeny. **F** Depiction of normal and elevated geothermal gradient curve and its effect on melt generation. **G** Stages of progressive anatexis in migmatite and associated granite melt generation with reference to decreasing dihedral angle between solid and melt phases

During the onset of deformation, the crust attained about 15 km thickness and thus schistosity started developing with different styles of folding (Fig. 15B). Subsequently, the gneissosity also generated with further growth of continent and associated thickness increase (i.e., depth and pressure increase). Meanwhile short-term changes in deformation (viz. faulting related uplift and isothermal decompression) and other factors can influence melting point to produce patchy migmatites. At the terminal Archaean, the crustal thickness and associated deformation was enough to form granitic melt of sufficient quantity to form batholith as per the pressure–temperature condition of ~30 km crust (Fig. 15C). P–T conditions from north (400 MPa–450 °C) to south (800 MPa–800 °C) in DC also supports the qualitative observation.

Possibly, a dynamo-thermal metamorphic setting with temperatures about ~600 °C can be deciphered from the gneissic rocks (Hefferan and O'Brien 2010). With further increase in depth and/or temperature the intense partial melting led to development of hybrid type of migmatitic rocks with both igneous and metamorphic characteristics (Sawyer

2008; Vernon 2004). Brittle structures developed mostly in the rocks of uppercrust resulting in widespread fracturing and faulting. Brittle-ductile boundary (Fig. 15D) or transitional regime structures are indicative of further deeper condition existing at ~10–20 km depth range and temperatures of about ~300 °C (Hefferan and O'Brien 2010). The temperatures at which transition from brittle to ductile behavior took place could not be the same for all minerals. For quartz this transition takes place at ~300 °C, for biotite ~250 °C, for feldspar ~400 °C, for amphibole and garnet ~650 °C (Passchier and Trouw 2005).

Rocks older than 3.4 Ga are not found in the EDC. However, progressive thickening of the Earth's crust from about 3 Ga to 2.5 Ga can be interpreted from the rock assemblages with characteristic structures and metamorphic signatures. Development of schistosity and gneissosity indicate a particular depth/thickness of crust, below which they cannot form. Since, the brittle-ductile transition zone (Duba 1990) occurs around 14–18 km depth range (Fig. 15D), it can be said that the presently observed ductile features like schistosity in greenstone belts, gneissic foliation and migmatitic rocks might have been formed during Meso to Neoproterozoic time when the crust in EDC achieved a thickness of at least about 25 km. The geothermal gradient of Earth was relatively steeper during Archaean because it was hotter. However, later concentration and enrichment of radioactive elements in the crust balances the net gradient. Therefore, the depth of formation of schistosity and gneissosity is related to accretionary growth of the crust because with progressive thickening of the crust geothermal gradient and pressure caused different types of burial and regional metamorphism and resultant fabrics.

Older schist/greenstone belts suggest 15–18 km thick crust which encountered initial deformation phases of Kenoran Orogeny (D_1 to D_4). In this way crust thickened with time and therefore pressure temperature condition also enhanced in the deeper part, which develop a prograde metamorphic track (Fig. 15E). Further, continued growth up to about 25 km when the gneissic fabric started appearing, deeper catazone part suffered anatexis and patchy migmatite pockets appeared (Fig. 15E; Duba 1990). With further thickening, rate of anatexis increased and drastic change in rheology occur due to enhanced melt proportion in the system. Thus, even low order deformation also could help in channelizing and segregating the melt. Therefore, when epizone part exhibited peak metamorphic condition, catazone parts got melted and such crustal melting generated small volumes of felsic magmas to form granite plutons but often



batholithic in dimensions and its upward transportation in the form of vein, apophyses in the mesozone also indicated along with simultaneous deformation (D_6). This deformation played significant role in granite migration and lower crustal melting by reducing melting point due to pressure release/decompression (Fig. 15F). Therefore, elevated geothermal gradient helped in granite melt generation and emplacement.

The formation of migmatites or granitoids by anatexis or partial melting are mainly influenced by two factors, viz. increasing pressure–temperature with progressive thickened crust (geothermal gradient) and deformation events. Finally, isothermal decompression with unloading, exhumation due to faulting exhibited a change from ductile to brittle regime (field 3 in Fig. 15A). These later brittle-ductile to pure brittle deformation events of post granite emplacement (D_7 onwards) belong to Hudsonian orogeny (Goswami et al. 2019b). Schist-gneiss-migmatites are developed in older ductile deformational regime (> 2.6 Ga Kenoran orogeny) unlike the younger granitoids with dominantly brittle deformational features (< 2.5 Ga Hudsonian orogeny) like fractures, veins, pseudotachylite and breccia (Goswami et al. 2021a, b).

Therefore, the present configuration of the EDC from north to south implies upliftment of southern part of northerly tilted crustal block. The uplifted southern part is eroded subsequently and fills the depression in the north as Kaladgi and Bhima basin sediments. Such deformation events can be understood from field data of epizone, mesozone and catazone rock assemblages, micro-structures and overgrowth textures as well as mineral assemblages. Petrographic observations also suggest hydration and brittle deformation features which are suggestive of decompression and upliftment to shallower depth. The process of granite batholith formation mechanism is shown in Fig. 15G.

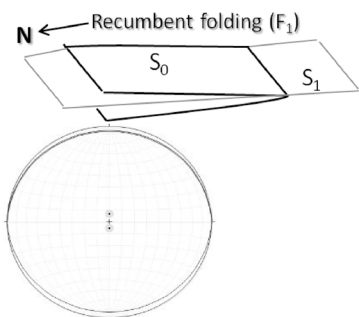
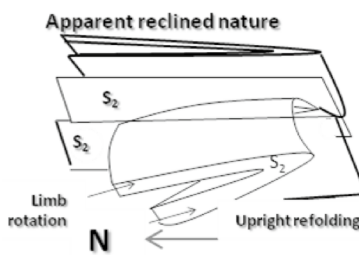
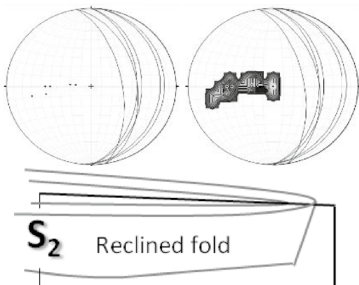
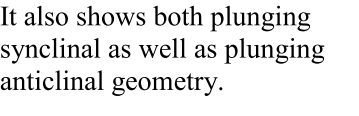
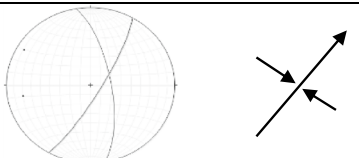
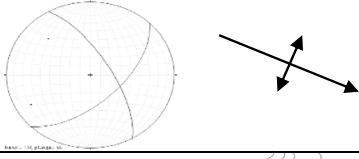
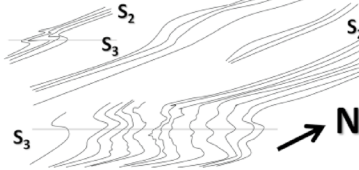
Conclusion

Based on the discussion and interpretation of all field data present study suggests the following broad conclusions:

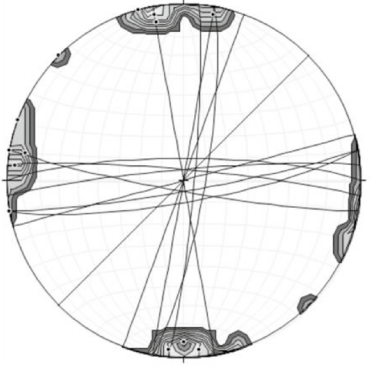
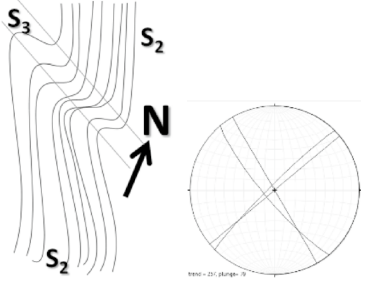
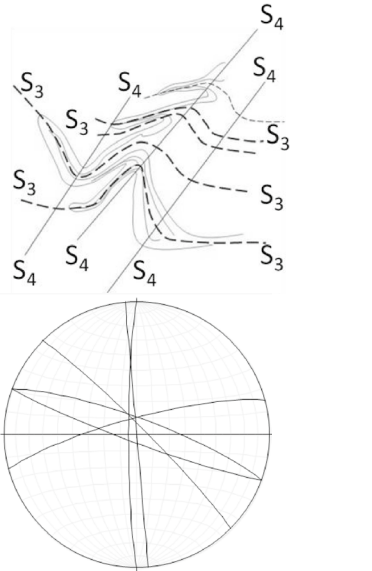

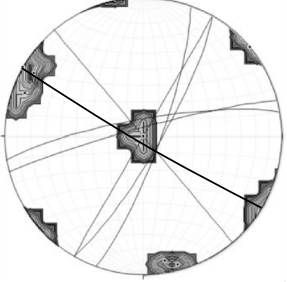
1. The different rock types in the EDC are genetically linked to the Archaean crust building process. The northern most part of the EDC is relatively less deformed than south. Northern part is characterized by K-feldspar rich granitoids with dominant brittle features such as faults with marked displacements, veination, pseudotachylite and dominant microcline megacrysts. The southernmost part is gneiss-migmatite rich ductile deformation dominated terrain. Presence of shear zones, mylonites, schistosity, gneissosity, migmatites of different types indicate anatexis and deformation fabrics. The granitoid and country rock contacts are also diffused in the south unlike the sharp contacts in the north.
2. This indicate a crustal epizone (< 10 km depth crust) in the north and catazone (> 15 km depth crust) in the south. The progressive change in litho-structural attributes (i.e., from epizone in the north through mesozone in the centre to catazone in the south) and grade of metamorphism (lower greenschist in north to upper amphibolite in south) from north to south indicate a preserved eroded segment of northerly tilted crust.
3. During the transition from ductile to brittle deformation regime of the overall system a significant tectonic event with signatures of brittle-ductile deformation (evidenced from protomylonites, reactivated shear zone and deformed en-echelon veins) have taken place during late Archaean.

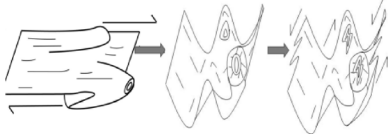
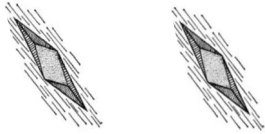
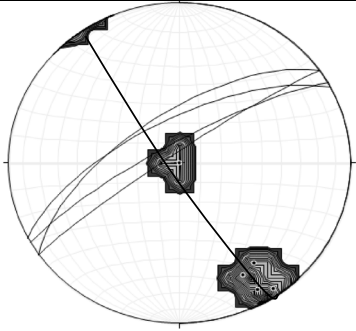
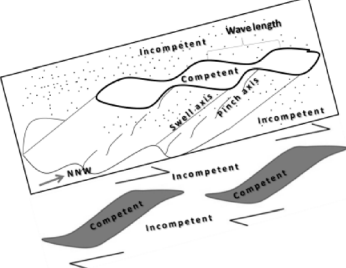
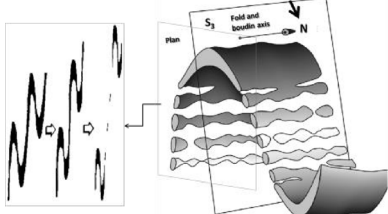
Annexure 1

Structural data sheet for schist, gneiss and migmatites

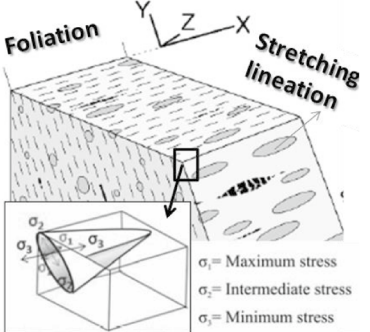
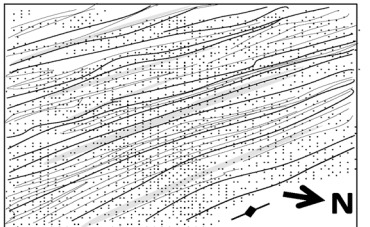
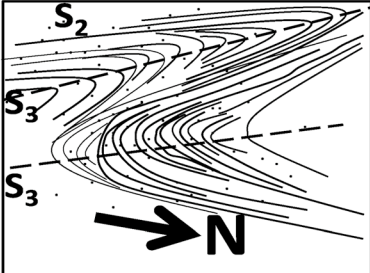
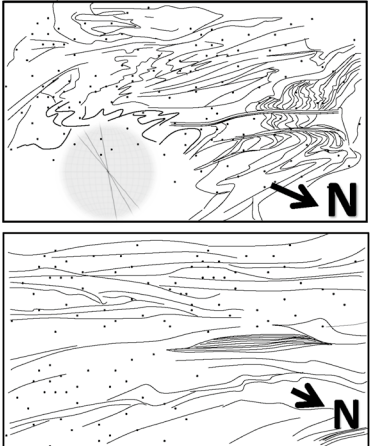
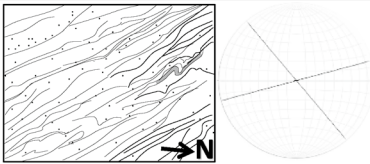
Rock type	Planar structure	Linear structure	Sketch representation
Schist	Recumbent fold with low dipping limbs (F_1) Limb 1 ($90^0/7^0 \rightarrow 180^0$) Limb 2 ($90^0/5^0 \rightarrow 0^0$) Axial plane $90^0/6^0 \rightarrow N$ First stage of deformation (D_1)	Sub-horizontal fold axis (E-W)	
Schist	Inclined fold axial plane, recliné plunging fold (older hinge area) Dip of axial planar foliation is $20^0 \rightarrow 90^0$	Pitch of axis on axial plane is 90^0 Plunge of fold axis varies from $10^0 \rightarrow 170^0$ to $5^0 \rightarrow 160^0$	
Schist	Inclined fold axial plane, recliné plunging fold (older hinge area) Dip of axial planar foliation is $60^0 \rightarrow 90^0$	Pitch of axis on axial plane is 90^0 Plunge of fold axis varies from $25^0 \rightarrow 155^0$ to $35^0 \rightarrow 135^0$	
Schist	Inclined fold axial plane, recliné plunging fold (older hinge area) Dip of axial planar foliation is $60^0 \rightarrow 90^0$	Pitch of axis on axial plane is 90^0 Plunge of fold axis varies from $45^0 \rightarrow 85^0$ to $55^0 \rightarrow 80^0$	
Schist	Recliné fold geometry with vertical N-S vertical axial plane (S_2) (older hinge area)	Pitch of axis on axial plane is 90^0 Plunge of fold axis is $80^0 \rightarrow 90^0$	It also shows both plunging synclinal as well as plunging anticlinal geometry.
Schist	Plunging syncline Limb 1 ($30^0/80^0 \rightarrow 120^0$) Limb 2 ($350^0/60^0 \rightarrow 80^0$) Axial plane $5^0/75^0 \rightarrow E$	Fold axis plunge $70^0 \rightarrow 60^0$ 2nd stage of deformation (D_2)	
Schist	Plunging anticline Limb 1 ($45^0/60^0 \rightarrow 135^0$) Limb 2 ($330^0/70^0 \rightarrow 60^0$) Axial plane $5^0/85^0 \rightarrow E$	Fold axis plunge $60^0 \rightarrow 115^0$ 2nd stage of deformation (D_2)	
Schist	Overtured and isoclinal fold (F_3) with axial plane (S_3) strike range from NNE to NNW and easterly dip ranging from 75^0 to 90^0	Fold axis is not plunging i.e., Vertical to sub-vertical. This is typical of 3rd stage of deformation	

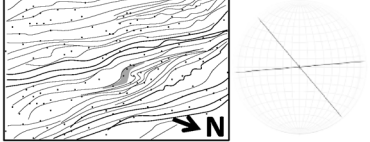
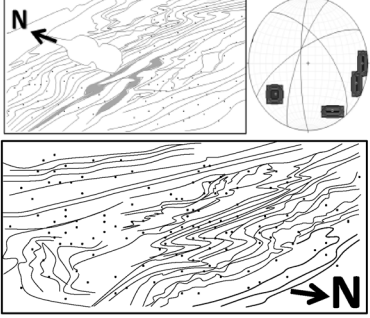
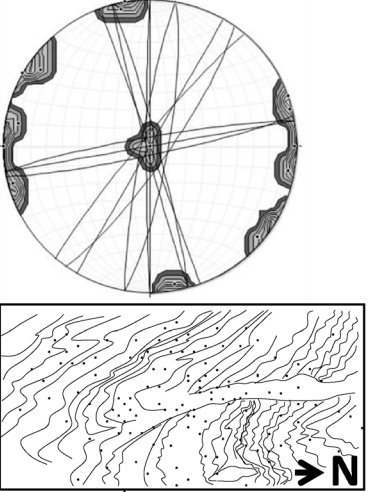


	<p>This 3rd stage of deformation (D_3) show refolded S_2 plane and different attitude at different parts e.g., N-S vertical, 350^0 vertical, 20^0 vertical, 10^0 vertical, $5^0/85^0 \rightarrow E$, $10^0/80^0 \rightarrow E$, $100^0/85^0 \rightarrow N$, $45^0/85^0 \rightarrow SE$, $85^0/80^0 \rightarrow N$, $80^0/85^0 \rightarrow S$, $85^0/85^0 \rightarrow S$</p>	<p>(D_3)</p>	
<p>Schist</p>	<p>Open fold (F_3) of 3rd stage deformation (D_3) with NW-SE sub-vertical axial plane (S_3). S_2 planes are refolded and attitude varies as follows: $140^0/80^0 \rightarrow 230^0$ 50^0 vertical, 150^0 vertical, $45^0/85^0 \rightarrow 315^0$</p>	<p>Fold axis plunge $80^0 \rightarrow 260^0$</p>	
<p>Schist</p>	<p>Quartz veins along S_2 plane were folded into tight to isoclinal folds (F_3). Refolded minor folds and tight folds (F_4) show variable range of north easterly axial planar direction. S_3 attitude varies as follows: $135^0/85^0 \rightarrow 45^0$ $75^0/80^0 \rightarrow 345^0$, 175^0 vertical, $110^0/85^0 \rightarrow 20^0$, $0^0/85^0 \rightarrow W$, E-W vertical. S_4 axial plane is mostly sub-vertical</p>	<p>Older (F_3) and younger (F_4) fold axes are parallel but axial planes are at high angle. Axes are mostly vertical to sub-vertical. Few areas show plunge of axes like $45^0 \rightarrow 357^0$, $75^0 \rightarrow 340^0$, $65^0 \rightarrow 280^0$, $70^0 \rightarrow 120^0$,</p>	
<p>Schist</p>	<p>Multiply deformed quartz vein with complicated refolded sheath folding. Here the horizontal plane of observation itself indicate rotation and folding. Variable direction of S_4 is already noted at different areas. The D_5 deformation and associated rotation gives</p>	 <p>Closed sub-circular outline indicate sheath fold development prior to rotation. Following</p>	 <p>Poles of presently observed folded S_4 planes indicate a major NW-SE</p>

	<p>apparently horizontal plane of observation and following attitudes.</p> <table border="1"> <thead> <tr> <th>Strike</th> <th>Dip</th> <th>Dip Quad</th> </tr> </thead> <tbody> <tr><td>030.0</td><td>90.0</td><td>E</td></tr> <tr><td>140.0</td><td>90.0</td><td>W</td></tr> <tr><td>020.0</td><td>80.0</td><td>E</td></tr> <tr><td>260.0</td><td>80.0</td><td>N</td></tr> <tr><td>255.0</td><td>85.0</td><td>N</td></tr> <tr><td>030.0</td><td>80.0</td><td>E</td></tr> <tr><td>000.0</td><td>00.0</td><td>E</td></tr> </tbody> </table>	Strike	Dip	Dip Quad	030.0	90.0	E	140.0	90.0	W	020.0	80.0	E	260.0	80.0	N	255.0	85.0	N	030.0	80.0	E	000.0	00.0	E	<p>plunge with trends are calculated</p> <table border="1"> <thead> <tr> <th>Trend</th> <th>Plunge</th> </tr> </thead> <tbody> <tr><td>300.0</td><td>00.0</td></tr> <tr><td>050.0</td><td>00.0</td></tr> <tr><td>290.0</td><td>10.0</td></tr> <tr><td>170.0</td><td>10.0</td></tr> <tr><td>165.0</td><td>05.0</td></tr> <tr><td>300.0</td><td>10.0</td></tr> <tr><td>270.0</td><td>90.0</td></tr> </tbody> </table>	Trend	Plunge	300.0	00.0	050.0	00.0	290.0	10.0	170.0	10.0	165.0	05.0	300.0	10.0	270.0	90.0	<p>strike of S₄ plane before rotation. Further D₆ deformation along major NNW older trend is rebuilt to exhibit shearing effects.</p> 
Strike	Dip	Dip Quad																																									
030.0	90.0	E																																									
140.0	90.0	W																																									
020.0	80.0	E																																									
260.0	80.0	N																																									
255.0	85.0	N																																									
030.0	80.0	E																																									
000.0	00.0	E																																									
Trend	Plunge																																										
300.0	00.0																																										
050.0	00.0																																										
290.0	10.0																																										
170.0	10.0																																										
165.0	05.0																																										
300.0	10.0																																										
270.0	90.0																																										
Schist	<p>Horizontal plan view nearby the schist-gneiss transition area containing symmetric pressure shadow lineation (L₃) indicate deformation (D₃)</p>	<p>Pressure shadow lineation is NNW-SSE trending and horizontal.</p>																																									
Schist	<p>Ptygmatic folding of sub-horizontal quartz vein (D₄) indicate upright folding (F₅) with thin limb thick hinge, indicate NNW-SSE compression (D₅). High competence contrast between vein and matrix material is notable. Isoclinal fold axial planes show 55°/65°→325° (S₅).</p>	<p>F₆ fold axis is sub-horizontal to gently plunging 10°→60°</p>																																									
Schist	<p>Pinch and swells (D₃) Symmetric type with NNW-SSE vertical competent layer. Asymmetric type show NNW-SSE vertical shear planes and NW-SE competent layers</p>	<p>Vertical pinch and swell axes for both symmetric and asymmetric types.</p>																																									
Schist	<p>Boudinaged fold Different parts are giving different fabrics and implying different fields of progressive stress. NNW-SSE vertical S₃ plane</p>	<p>Boudin axis and fold axis are vertical and parallel to each other. This is D₃ deformation event</p>																																									



Schist	S-Tectonites N-S vertical Brittle nature dominant Granite apophyses along weak foliation (S_6 and older) are stretched and broken to form tectonite	Stretching lineation (L-tectonites), N-S horizontal This is the transition from ductile to brittle regime (i.e., D_7)	
Gneiss	Lit-per-lit gneiss foliation 160^0 - 340^0 vertical	Horizontal 160^0 - 340^0 intersection lineation	
Gneiss	Tight reclined fold NNW - SSE strike of S_3 axial plane. Limb 1 (N-S/sub-vertical) Limb 2 (140^0 - 320^0 /sub-vertical)	Axis plunge $85^0 \rightarrow 270^0$	
Gneiss	Tight reclined fold NNW - SSE strike of S_3 axial plane. Limb 1 (170^0 - 350^0 /sub-vertical) Limb 2 (140^0 - 320^0 /sub-vertical). S_3 foliation along axial plane indicate transposition and material flow. Initial stage of migmatite development is recognizable	No plunge is possible to determined from plan. Schlieren oriented along 150^0 - 330^0 trend.	
Gneiss	140^0 - 320^0 /sub-vertical gneissic foliation, 'Z' fold and 'S' fold indicate some particular limb parts of larger scale fold. "Z" fold Limb 1 (75^0 - 255^0 /sub-vertical) Limb 2 (140^0 - 320^0 /sub-vertical).	Vertical fold axis	

	<p>"S" fold Limb 1 (85°-255° /sub-vertical) Limb 2 (140°-320° /sub-vertical).</p>																																																																													
<p>Gneiss</p>	<p>"S" fold Limb 1 ($140^{\circ}/60^{\circ} \rightarrow 50^{\circ}$) Limb 2 ($60^{\circ}/70^{\circ} \rightarrow 330^{\circ}$). Limb 1 ($140^{\circ}/60^{\circ} \rightarrow 50^{\circ}$) Limb 2 ($20^{\circ}/75^{\circ} \rightarrow 290^{\circ}$). Limb 1 ($145^{\circ}/60^{\circ} \rightarrow 55^{\circ}$) Limb 2 ($20^{\circ}/75^{\circ} \rightarrow 290^{\circ}$). Tight chevron fold Limb 1 ($150^{\circ}/80^{\circ} \rightarrow 55^{\circ}$) Limb 2 ($165^{\circ}$/vertical). Axial plane 155°/vertical</p>	<p>Axis plunge $58^{\circ} \rightarrow 24^{\circ}$ Axis plunge $49^{\circ} \rightarrow 2^{\circ}$ Axis plunge $55^{\circ} \rightarrow 345^{\circ}$</p>																																																																												
<p>Gneiss</p>	<p>160°-340°/sub-vertical wide channel along axial planar directions of major folds and flowage along minor fold limbs. Migmatite stage with intense folding and granite melt generation and segregation (D_6)</p> <table border="1" data-bbox="357 1037 647 1339"> <thead> <tr> <th>Strike</th> <th>Dip</th> <th>Dip Quad</th> </tr> </thead> <tbody> <tr><td>160.0</td><td>90.0</td><td>W</td></tr> <tr><td>030.0</td><td>90.0</td><td>E</td></tr> <tr><td>000.0</td><td>90.0</td><td>E</td></tr> <tr><td>010.0</td><td>80.0</td><td>E</td></tr> <tr><td>190.0</td><td>85.0</td><td>W</td></tr> <tr><td>165.0</td><td>88.0</td><td>W</td></tr> <tr><td>345.0</td><td>86.0</td><td>E</td></tr> <tr><td>035.0</td><td>80.0</td><td>E</td></tr> <tr><td>220.0</td><td>85.0</td><td>W</td></tr> <tr><td>180.0</td><td>88.0</td><td>W</td></tr> <tr><td>080.0</td><td>90.0</td><td>S</td></tr> <tr><td>078.0</td><td>85.0</td><td>S</td></tr> <tr><td>260.0</td><td>85.0</td><td>N</td></tr> <tr><td>000.0</td><td>00.0</td><td>E</td></tr> </tbody> </table>	Strike	Dip	Dip Quad	160.0	90.0	W	030.0	90.0	E	000.0	90.0	E	010.0	80.0	E	190.0	85.0	W	165.0	88.0	W	345.0	86.0	E	035.0	80.0	E	220.0	85.0	W	180.0	88.0	W	080.0	90.0	S	078.0	85.0	S	260.0	85.0	N	000.0	00.0	E	<p>Pole data</p> <table border="1" data-bbox="692 783 916 1184"> <thead> <tr> <th>Trend</th> <th>Plunge</th> </tr> </thead> <tbody> <tr><td>070.0</td><td>00.0</td></tr> <tr><td>300.0</td><td>00.0</td></tr> <tr><td>270.0</td><td>00.0</td></tr> <tr><td>280.0</td><td>10.0</td></tr> <tr><td>100.0</td><td>05.0</td></tr> <tr><td>075.0</td><td>02.0</td></tr> <tr><td>255.0</td><td>04.0</td></tr> <tr><td>305.0</td><td>10.0</td></tr> <tr><td>130.0</td><td>05.0</td></tr> <tr><td>090.0</td><td>02.0</td></tr> <tr><td>350.0</td><td>00.0</td></tr> <tr><td>348.0</td><td>05.0</td></tr> <tr><td>170.0</td><td>05.0</td></tr> <tr><td>270.0</td><td>90.0</td></tr> </tbody> </table>	Trend	Plunge	070.0	00.0	300.0	00.0	270.0	00.0	280.0	10.0	100.0	05.0	075.0	02.0	255.0	04.0	305.0	10.0	130.0	05.0	090.0	02.0	350.0	00.0	348.0	05.0	170.0	05.0	270.0	90.0	
Strike	Dip	Dip Quad																																																																												
160.0	90.0	W																																																																												
030.0	90.0	E																																																																												
000.0	90.0	E																																																																												
010.0	80.0	E																																																																												
190.0	85.0	W																																																																												
165.0	88.0	W																																																																												
345.0	86.0	E																																																																												
035.0	80.0	E																																																																												
220.0	85.0	W																																																																												
180.0	88.0	W																																																																												
080.0	90.0	S																																																																												
078.0	85.0	S																																																																												
260.0	85.0	N																																																																												
000.0	00.0	E																																																																												
Trend	Plunge																																																																													
070.0	00.0																																																																													
300.0	00.0																																																																													
270.0	00.0																																																																													
280.0	10.0																																																																													
100.0	05.0																																																																													
075.0	02.0																																																																													
255.0	04.0																																																																													
305.0	10.0																																																																													
130.0	05.0																																																																													
090.0	02.0																																																																													
350.0	00.0																																																																													
348.0	05.0																																																																													
170.0	05.0																																																																													
270.0	90.0																																																																													



Annexure 2

Deformation episodes and corresponding structure in different lithounits

Deformation stage	Major events	Nature of deformation	Description	Remarks
D ₁ (Ductile)	Recumbent folding (F ₁)	Most prominent in the form of horizontal (S ₁) axial plane in greenstone belt along epizone-mesozone part	This is oldest event of deformation, often disturbed by later imprints. This stage is better manifested in the northern (epizone-mesozone) and central part of EDC schist belts	Obscure in TTG gneiss and migmatite
D ₂ (Ductile)	Upright folding (F ₂)	Most prominent in the form of vertical (S ₂) axial plane in greenstone belt along epizone-mesozone part	Rotation of older (S ₁) axial plane is visible at places near the older hinge portion, where limbs become tight to isoclinal with apparent reclined plunging as well as non-plunging neutral geometry	Quartz veination started along this newly developed NNW-SSE to N-S (S ₂) planes. Onset of lit-per-lit gneiss generation
D ₃ (Ductile)	Tight to isoclinal folding with layer parallel slip	Most prominent in the form of vertical NNW to NW striking axial plane (S ₃) in greenstone belt and gneiss-migmatite along all the parts (i.e., epi, meso and catazone)	Older (S ₂) layer parallel slip produced intrafolial folding of neutral tight to isoclinal fold with most commonly NNW and NNE striking sub-vertical axial plane (S ₃). Thick hinge thin limb style of folding in common in both gneiss and schist of mesozone and catazone. Differential flowage of older quartz vein is common due to layer parallel transposition., stretching and leucocratic flow from fold limb towards hinge part. Boudinage is common along with folding	This stage is equally abundant in gneiss and schist belts with broadly NNW sub-vertical axial plane. Pressure shadow lineation developed at some places. Gneissosity development by differential flow, leucocratic and melanocratic banding. Patchy migmatites with isolated melt pockets developed with high solid-melt dihedral angle ($\theta > 60^\circ$)
D ₄ (Ductile)	Type3 interference folding (F ₄) over older (S ₃) planes, sheath folding in quartz vein	Commonly found in the southern block (catazone), where complicated deformation fabrics often show intense overlapping	Different parts of quartz vein show different nature. Relative orientation with reference to the stress direction and its major shearing component give different signatures at different area. Migmatite development is abundant and immensely controlled by the weak channel development along shear bands in the southern part (catazone)	Development of minor "S" and "Z" fold as part of opposite limbs of major fold in gneiss, sheath fold in quartz veins within schist belt due to competence contrast. Stromatic and other migmatite developed along linear channel. Dihedral angle reduced with increase in melt fraction

Deformation stage	Major events	Nature of deformation	Description	Remarks
D ₅ (Ductile)	Rotation of sheath fold head by probable upright fold (F ₅)	This upright fold axial plane (S ₅) is rarely observed in the southern part (catazone) at high angle to the general NNW trend	This stage is giving us opportunity to observe sub-circular sheath fold outline in plan. The high angle (> 60°) between general NNW foliation and S ₅ is giving vertical to sub-vertical intersection lineation. Granite generation from diatexite started because generation of about 25% melt can form interlinking melt network. Transition from solid dominated to melt dominated mass. In this system slight deformation can play significant role in creating melt migration channel	Older horizontal folded veins exhibit upright folding in section view also. Percentage of melt increases to the south, i.e., deeper crust segment. The system in the southern extreme become juvenile granite melt dominated rock mass. The drastic change in rheology of the system lead to form gradational contact between solid and melt phase
D ₆ (Ductile)	Refolding parallel to older dominant NNW trend	Plan outcrop of deformed folded sheath fold is indicating this event	This event is significant in the catazone and mesozone for segregation and transportation of granitic melt. Granitic apophyses and tongues are common	This is considerable as reactivation of older shear zone, which facilitate upward movement of juvenile granite melt
D ₇ (Brittle-ductile transition)	L-S tectonites	Transition stage with exhumation by faulting and associated block upliftment, possible tilting and unloading	Granitic vein/apophyses within metabasics of greenstone belt create competence contrast. Stretching lead to elliptical fragmentation and alignment normal to E-W maximum compression (σ ₁)	This is the first deformation as post granite emplacement
Later brittle deformation stages	Mostly post Archaean events	Pure brittle deformation	Mafic dyke swarms, quartz vein-reef, faulting and reactivation etc. followed by Proterozoic basin opening	These events are not addressed in detail in the present context

Acknowledgements We express our sincere gratitude to the editor, reviewers for suggestion and encouragement. Sincere thanks to the in-charge Publication group and Director AMD for encouragement, support and guidance.

Data availability All data are presented in the paper. There is no additional data available.

Declarations

Competing Interests It is declared that the paper titled Implication of deformation fabrics of schist-migmatite-gneiss and granite in understanding regional tectonics: Eastern Dharwar Craton (EDC), India, authored by Sukanta Goswami*, Sangeeta Bhagat, Dheeraj Pande, D. K. Choudhury, B. Saravanan and D. K. Sinha is not submitted elsewhere and not ever published even partially before. All the information is new and based on present work. There is no conflict of interest involved with the work. There is no financial interests and no direct or indirect relation involved to the work submitted for publication. The field based work is a part of regular assigned works without any financial support from any organization.

References

Belica, M.E., Piispa, E.J., Meert, J.G., Pesonen, L.J., Plado, J., Pandit, M.K., Kamenov, G.D., Celestino, M.: Paleoproterozoic mafic dyke swarms from the Dharwar craton; paleomagnetic poles for India from 2.37 to 1.88 Ga and rethinking the Columbia supercontinent. *Precamb. Res.* **244**, 100–122 (2014)

Bhaskar Rao, Y.J., Vijaya Kumar, T., Sreenivas, B., Babu, E.V.S.S.K.: A Review of Paleo- to Neoproterozoic crustal evolution in the Dharwar craton, Southern India and the transition towards a Plate Tectonic regime. *Episodes* **43**(1), 51–68 (2020)

Bidyananda, M., Goswami, J.N., Srinivasan, R.: Pb-Pb zircon ages of Archaean metasediments and gneisses from the Dharwar Craton, southern India: implications for the antiquity of the eastern Dharwar Craton. *Journal of Earth Systems Science* **120**, 643–661 (2011)

Chadwick, B., Vasudev, V.N., Ahmed, N.: The Sandur schist belt and its adjacent plutonic rocks: implications for late archaean crustal evolution in Karnataka. *J. Geol. Soc. India* **47**, 37–57 (1996)



- Chadwick, B., Vasudevan, V.N., Hegde, G.V.: The Dharwar craton, southern India, interpreted as the result of Late Archaean oblique convergence. *Precamb. Res.* **99**, 91–111 (2000)
- Chadwick, B., Vasudevan, V.N., Hegde, G.V., Nutman, A.P.: Structure and SHRIMP U/Pb zircon ages of granites adjacent to the Chitradurga schist belt: Implications for Neoproterozoic convergence in the Dharwar craton, southern India. *J. Geol. Soc. India* **69**, 5–24 (2007)
- Chardon, D., Peucat, J.J., Jayananda, M., Choukroune, P., Fanning, C.M.: Archean granite-greenstone tectonics at Kolar (South India): interplay of diapirism and bulk inhomogeneous contraction during juvenile magmatic accretion. *Tectonics* **21**, 10–16 (2002)
- Chardon, D., Jayananda, M.: Three-dimensional field perspective on deformation, flow, and growth of the lower continental crust (Dharwar Craton, India); *Tectonics*, 27p. TC1014 (2008)
- Chardon, D., Jayananda, M., Peucat, J.J.: Lateral contractional flow of hot orogenic crust: insights from the Neoproterozoic of South India, geological and geophysical implications for orogenic plateau. *Geochem. Geophys. Geosyst.* **12**, Q02005 (2011)
- Dey, S., Pandey, U.K., Rai, A.K., Chaki, A.: Geochemical and Nd isotope constraints on petrogenesis of granitoids from NW part of the eastern Dharwar craton: possible implications for late Archaean crustal accretion. *J. Asian Earth Sci.* **45**, 40–56 (2012)
- Dey, S.: Evolution of Archaean crust in the Dharwar craton: the Nd isotope record. *Precamb. Res.* **227**, 227–246 (2013)
- Dey, S., Halla, J., Kurhila, M., Nandy, J., Heilimo, E., Pal, S.: Geochronology of Neoproterozoic granitoids of the NW eastern Dharwar craton: implications for crust formation. *Geol. Soc. Lond. Spec. Publ.* **449**(1), 89–121 (2016)
- Drury, S.A., Holt, R.W.: The tectonic framework of the south India craton: a reconnaissance involving LANDSAT imagery. *Tectonophysics* **65**, 111–115 (1980)
- Duba, A.G.: The brittle-ductile transition in rocks: the heard volume. *Am. Geophys. Union* **56**, 243p (1990)
- French, J., Heaman, L.M.: Precise U-Pb dating of Paleoproterozoic mafic dyke swarms of the Dharwar craton, India: Implications for the existence of the Neoproterozoic supercraton Sclavia. *Precamb. Res.* **183**, 416–441 (2010)
- Gireesh, R.V., Sekhmo, K., Jayananda, M.: Anatomy of 2.57–2.52 Ga granitoid plutons in the eastern Dharwar craton, southern India: implications for magma chamber processes and crustal evolution. *Episodes* **35**(3), 398–413 (2012)
- Goscombe, B.D., Passchier, C.W., Hand, M.: Boudinage classification: end-member boudin types and modified boudin structures. *J. Struct. Geol.* **26**(4), 739–763 (2004)
- Goswami, S., Sivasubramanian, R., Bhagat, S., Suresh, K., Sarbajna, C.: Algoma type BIF and associated submarine volcanosedimentary sequence in Ramagiri granite-greenstone terrain, Andhra Pradesh, India. *J. Appl. Geochem.* **18**(2), 155–169 (2016)
- Goswami, S., Upadhyay, P.K., Bhattacharjee, P., Murugan, M.G.: Tectonic setting of the Kadiri schist belt, Andhra Pradesh, India. *Acta Geol. Sin. Engl. Ed.* **91**(6), 1992–2006 (2017)
- Goswami, S., Tiwari, R.P., Maurya, V.K., Natarajan, V., Saravanan, B., Bhatt, A.K., Verma, M.B.: Potentiality of uranium mineralisation along NE-SW trending Sivaramapuram-Nutanakalva fracture zone in basement granitoids, Kadapa basin, Andhra Pradesh, India. *J. Appl. Geochem.* **21**(1), 55–64 (2019a)
- Goswami, S., Maurya, V.K., Tiwari, R.P., Swain, S., Verma, M.B.: Structural analysis of T. Sundupalle greenstone belt and surrounding granitoids, Andhra Pradesh, India. *Arab. J. Geosci.* (2019). <https://doi.org/10.1007/s12517-019-4793-2>
- Goswami, S., Bhattacharjee, P., Swain, S., Sarbajna, C., Muralidharan, R., Choudhury, D.K., Pande, D., Sinha, D.K.: Migmatite rheology of crustal catatone: an example from the SSE part of T. Sundupalle granite-greenstone terrain, Eastern Dharwar Craton, India. *Geol. J.* **56**(4), 10 (2021). <https://doi.org/10.1002/gj.4159>
- Goswami, S., Tiwari, R.P., Maurya, V.K., Natarajan, V., Saravanan, B., Bhatt, A.K., Verma, M.B.: Exploration for concealed fracture-controlled uranium mineralization: a case from Shivaramapuram-Nutanakalva tract in basement granitoids, south of Cuddapah basin, Andhra Pradesh, India. *J. Geochem. Explor.* **226**, 6710 (2021). <https://doi.org/10.1016/j.gexplo.2020.106710>
- Gupta, S., Rai, S.S., Prakasam, K.S., Srinagesh, D., Bansal, B.K., Chadha, R.K., Priestley, K., Gaur, K.: The nature of the crust in southern India: implications for Precambrian crustal evolution. *Geophys. Res. Lett.* **30**, 10 (2003). <https://doi.org/10.1029/2002GL016770>
- Hefferan, K., O'Brien, J.: *Earth Materials*, p. 670. John Wiley & Sons Ltd., Wiley-Blackwell, London (2010)
- Jayananda, M., Moyen, J.F., Martin, H., Peucat, J.J., Auvray, B., Mahabaleswar, B.: Late Archean (2550–2520 Ma) juvenile magmatism in the eastern Dharwar craton, southern India: constraints from geochronology, Nd-Sr isotopes and whole rock geochemistry. *Precamb. Res.* **99**, 225–254 (2000)
- Jayananda, M., Chardon, D., Peucat, J.J., Capdevila, R.: 2.61 Ga potassic granites and crustal reworking in the western Dharwar craton, southern India: tectonic, geochronologic and geochemical constraints. *Precamb. Res.* **150**, 1–26 (2006)
- Jayananda, M., Banerjee, M., Pant, N.C., Dasgupta, S., Kano, T., Mahesha, N., Mahabaleswar, B.: 2.62 Ga high-temperature metamorphism in the central part of the Eastern Dharwar Craton: implications for late Archaean tectonothermal history. *Geol. J.* **27**(2–3), 213–236 (2011). <https://doi.org/10.1002/gj.1308>
- Jayananda, M., Peucat, J.J., Chardon, D., Krishna Rao, B., Fanning, C.M., Corfu, F.: Neoproterozoic greenstone volcanism and continental growth, Dharwar Craton, southern India: constraints from SIMS U-Pb zircon geochronology and Nd isotopes. *Precamb. Res.* **227**, 55–76 (2013)
- Jayananda, M., Chardon, D., Peucat, J.J., Tushipokla, F.C.M.: Paleo- to Mesoproterozoic TTG accretion and continental growth in the western Dharwar Craton, Southern India: Constraints from SHRIMP U-Pb zircon geochronology, whole-rock geochemistry and Nd-Sr isotopes. *Precamb. Res.* **268**, 295–322 (2015)
- Jayananda, M., Santosh, M., Aadhisheshan, K.R.: Formation of Archean (3600–2500 Ma) continental crust in the Dharwar Craton, southern India. *Earth-Science Reviews*, p. 181 (2018)
- Jayananda, M., Aadhisheshan, K.R., Kusiak, M.A., Wilde, S., Sekhmo, K., Guitreau, M., Santosh, M., Gireesh, R.V.: Multi-stage crustal growth and Neoproterozoic geodynamics in the Eastern Dharwar Craton, Southern India. *Gondwana Res.* (2020). <https://doi.org/10.1016/j.gr.2019.09.005>
- Jayananda, M., Guitreau, M., Aadhisheshan, K.R., Miyazaki, T., Chung, S.L.: Origin of the oldest (3600–3200 Ma) cratonic core in the Western Dharwar Craton, Southern India: Implications for evolving tectonics of the Archean Earth. *Earth Sci. Rev.* **236**, 104278 (2023)
- Katz, M.B.: The tectonics of Precambrian craton—mobile belts: progressive deformation of polygonal miniplates. *Precamb. Res.* **27**(4), 307–319 (1985)
- Li, S.S., Santosh, M., Palin, R.M.: Metamorphism 1769 during the Archean–proterozoic transition associated with micro-block amalgamation in the Dharwar craton, India. *J. Petrol.* **59**(12), 2435–2462 (2018a)
- Li, S.S., Santosh, M., Ganguly, S., Thanooja, P.V., Sajeev, K., Pahari, A. et al.: Neoproterozoic microblock amalgamation in southern India: evidence from the nallamalaisuture zone. *Precambrian Res.* (2018b). S030192681830127X.
- Maibam, B., Goswami, J.N., Srinivasan, R.: Pb–Pb zircon ages of Archaean metasediments and gneisses from the Dharwar craton,



- southern India: implications for the antiquity of the eastern Dharwar craton. *J. Earth Syst. Sci.* **120**, 643–661 (2011)
- Manikyamba, C., Kerrich, R.: Eastern Dharwar Craton, India: Continental lithosphere growth by accretion of diverse plume and arc terranes. *Geosci. Front.* **3**(3), 225–240 (2012)
- Manikyamba, C., Ganguly, S., Santosh, M., Subramanyam, K.S.V.: Volcano-sedimentary and metallogenic records of the Dharwar greenstone terranes, India: Window to Archean plate tectonics, continent growth, and mineral endowment. *Gondwana Research* **50p** (2017)
- Moyen, J.F., Jayananda, M., Nedelec, A., Martin, H., Mahabaleswar, B., Auvray, B.: From the roots to the roof of a granite: the closepet granite of South India. *J. Geol. Soc. India* **62**(6), 753–768 (2003)
- Naqvi, S.M., Rogers, J.W.: Precambrian geology of India, Oxford University Press, New York, Monographs on Geology and Geophysics memoir, 6, 223 p. (1987)
- Nelson, S.A.: Types of metamorphism, Lecture notes. Tulane University. <https://www.tulane.edu> (2018)
- Newton, R.C.: The late Archean high-grade terrain of South India and the deep structure of the Dharwar Craton. In: Salisbury, M.H., Fountain, D.M. (eds.) *Exposed Cross-Sections of the Continental Crust*, pp. 305–326. Kluwer Academic Publishers, Amsterdam (1990)
- Pichamuthu, C.S., Srinivasan, R., Fareeduddin, Bhasker, A.A.: Archean crustal thickness of greenstone granite belts of South India. *Proc. Indian Acad. Sci. (Earth Planet. Sci.)* **90**(3), 217–226 (1981)
- Passchier, C.W., Trouw, R.A.J.: *Microtectonics*, 2nd edn., p. 366p. Springer, New York (2005)
- Jayananda, M., Peucat, J.J., Chardon, D., Rao, B.K., Fanning, C.M., Corfu, F.: The lower crust of Dharwar craton, south India: patchwork of Archean granulitic domains. *Precambrian Res.* **227**, 4–29 (2013). <https://doi.org/10.1016/j.precamres.2012.06.009>
- Poirier, J.P.: *Creep of Crystals*, p. 260. Cambridge University Press, Cambridge (1985)
- Radhakrishna, B.P., Naqvi, S.M.: Precambrian continental crust of India and its evolution. *J. Geol.* **94**, 145–166 (1986)
- Ramsay, J.G.: *Folding and Fracturing of Rocks*, p. 568. McGraw-Hill, New York (1967)
- Ramsay, J.G., Huber, M.I.: *The Techniques of Modern Structural Geology. 2. Folds and Fractures*, p. 406p. Academic Press, London (1987)
- Rogers, J.J.W.: The Dharwar Craton and the assembly of Peninsular India. *J. Geol.* **94**, 129–143 (1986)
- Sawyer, E.W.: *Atlas of Migmatites*, p. 385p. Special Publication, National Research Council Canada and Mineralogical Association of Canada (2008)
- Soderlund, U., Bleeker, W., Demirer, K., Srivastava, R.K., Hamilton, M.A., Nilsson, M.K.M., et al.: Emplacement ages of Paleoproterozoic mafic dyke swarms in eastern Dharwar craton, India: Implications for paleoreconstructions and support for a ~30° change in dyke trends from south to north. *Precamb. Res.* **329**, 26–43 (2019)
- Swami Nath, J., Ramakrishnan, M., Viswanatha, M.N.: Dharwarstratigraphic model and Karnataka eraton evolution. *Geol. Surv. India Rec.* **7**, 149–175 (1976)
- Swami Nath, J., Ramakrishnan, M.: The early Precambrian supracrustals of southern Karnataka. *Geological Survey of India. Memoir*, 112, 350 p (1981)
- Taylor, S.R., McLennan, S.M.: The composition and evolution of the continental crust: rare earth element evidence from sedimentary rocks. *Philos. Trans. R. Soc.* **A288**, 381–399 (1981)
- Taylor, S.R., Mc Lennan, S.M.: *Planetary Crusts: Their composition, origin and evolution*. Cambridge University Press The Edinburgh Building, Cambridge CB2 8RU, UK (2009). ISBN-13 978-0-511-46382-2
- Urai JL, Means WD, Lister GS (1986) Dynamic recrystallization of minerals. In: *Mineral and rock deformation: laboratory studies. The Paterson volume*, 161–199.
- Vanderhaeghe, O.: Migmatites, granites and orogeny: flow modes of partially-molten rocks and magmas associated with melt/solid segregation in orogenic belts. *Tectonophysics* **477**, 119–134 (2009)
- Vernon, R.H.: *Metamorphic Processes; Reactions and Microstructure Development*, p. 247. Allen Unwin, London (1983)
- Vernon, R.H.: *A Practical Guide to Rock Microstructure*, p. 650p. Cambridge University Press, Cambridge (2004)
- Vijaya, R.V., Damodara, N., Sain, K., Sen, M.A.S.N., Sarkar, D.: Upper crust of the Archean Dharwar craton in southern India using seismic refraction tomography and its geotectonic implications. *Geophys. J. Int.* **200**, 652–663 (2015)
- Viswanatha, M.N., Ramakrishnan, M.: The pre-Dharwar supracrustal rocks of Sargur Schist Complex in southern Karnataka and their tectonometamorphic significance. *Indian Mineral* **16**, 48–65 (1976)

Springer Nature or its licensor (e.g. a society or other partner) holds exclusive rights to this article under a publishing agreement with the author(s) or other rightsholder(s); author self-archiving of the accepted manuscript version of this article is solely governed by the terms of such publishing agreement and applicable law.

